Calculations on a boiling water fractor as a test of the Risø reactor code complex

Larsen, Anne Margrethe Hvidtfeldt; Larsen, Hans Hvidtfeldt; Petersen, T.

Publication date:
1972

Document Version
Publisher's PDF, also known as Version of record

Risø Report No. 268

Risø Report No. 268

Danish Atomic Energy Commission

Research Establishment Risø

Calculations on a Boiling Water Reactor as a Test of the Risø Reactor Code Complex

by A. M. Hvidtfeldt Larsen, H. Larsen and T. Petersen

June 1972

Sales distributors: Jul. Gjellerup, 87, Sølvgade, DK-1307 Copenhagen K, Denmark

Available on exchange from: Library, Danish Atomic Energy Commission, Risø, DK-4000 Roskilde, Denmark

June 1972 Risø Report No. 268

Calculations on a Boiling Water Reactor as a Test of the Risø Reactor Code Complex

by

A. M. Hvidtfeldt Larsen, H. Larsen and T. Petersen

Danish Atomic Energy Commission
Research Establishment Risø
Reactor Physics Department

Abstract

The boiling water reactor calculation methods used at Risø are described. A series of test calculations performed on the DRESDEN 1 reactor is presented. The code system used span the area from 76-group isotopic cross sections via box calculations to three-dimensional overall calculations inclusive of the void and temperature distributions.

CONTENTS

		Page
1.	Introduction	5
2.	Description of the DRESDEN 1 Reactor	5
3.	Cross Sections	13
	3.1. Energy Group Structures	13
	3.2. 10-Group Cross Sections for Burn-up Calculations	16
	3.3. 5- and 2-Group Cross Sections for Non-burnable Regions	19
4.	Unit Cell Burn-up Investigations	26
	4.1. Description of Unit Cell Calculations	26
	4.2. Strategy in Unit Cell Data Supply for Box Calculations	36
5.	Fuel Box Calculations	37
	5.1. Description of the Box Calculations	38
	5.2. Comparisons with Other Calculations	41
	5.3. Comparisons with Measurements	45
6.	Control Rods	56
	6.1. Cross Sections for Control Rods	56
	6.2. S_4 Calculations	58
	6.3. Diffusion Calculations	59
	6.4. Results	59
	6.5. Conclusion	61
7.	SYNTRON/VOID a Three-Dimensional Overall Burn-up Program	61
8.	Hydraulics	66
	8.1. Flow in a Single Vertical Channel	66
	8.2. Models for Boiling and Heat Transfer	68
	8.3. Numerical Solution	70
	8.4. Hydraulics Calculation for the Core	72
	8.5. The Fuel Model	74
9.	Homogenized Box Cross Sections for the Overall Calculations.	75

Commonwealth Edison Company
Chicago, Ill.

	Page
9.1. Construction of the Cross Section Tables	76
9.2. Fuel Temperature Dependence, Doppler Effect	79
9.3. Fuel Temperature and Void Coefficients	82
10. 3D Overall Calculations on the DRESDEN 1 Reactor	83
10.1. Initial Calculations, Approach to Criticality	84
10.2. 3D Burn-up Calculations on the First Cycle of the DRESDEN 1 Reactor	93
11. Conclusion	99
Acknowledgements	99
References	100

1. INTRODUCTION

This report describes the methods used for stationary and quasi-stationary boiling water reactor calculations at Risø. Moreover, a series of test calculations performed on the DRESDEN 1 reactor is presented.

The code system used span the area from 76-group isotopic cross sections to three-dimensional overall calculations inclusive of the void and temperature distributions. The Risø 76-group cross section system is rather new and based on fundamental nuclear data. This data system supplies the box code with collapsed, typically 10-group, cross sections. Box calculations are performed in order to find the isotopic composition as a function of the burn-up for the different pin locations in the box; moreover, the box code supplies the overall code with few-group macroscopic homogenized box cross sections. The three-dimensional overall calculations are based on a flux synthesis program including routines for calculation of the void and temperature distributions in the reactor core.

To perform test calculations with this program complex, the DRESDEN 1 reactor was chosen. Only few measurements on boiling water reactors are available in the literature. For the DRESDEN 1 reactor, however, the following measurements are available: some detailed box burn-up measurements 0-20 000 MWD/TU; initial critical control rod configurations, cold and hot; a few power distribution measurements; and the box average exposure distribution end of cycle 1. On the basis of such integral measurements it is not possible to test the individual programs one by one, but only the whole complex simultaneously. For example a 3D full power calculation involves uncertainties from the void calculation, the flux synthesis approximation, the box calculation, the cross sections and so on.

Parts of the program complex have been used previously for calculations on the Yankee reactor[1]. But in these calculations, the data generating system and the 3D program were not yet operational. Concurrently with the DRESDEN 1 calculations, the program complex is for the moment used for test calculations on the Connecticut Yankee reactor.

2. DESCRIPTION OF THE DRESDEN 1 REACTOR

The DRESDEN 1 is a boiling water reactor of 180 MW electric and 620 MW thermal. The reactor is built by General Electric Company for the Commonwealth Edison Company. It is situated 50 miles southwest of Chicago, Ill. The reactor was first critical in October 1959 and on full

power operation in June 1960.

The reactor is light water moderated and cooled. In the calculations described in this report only the first core was investigated, and therefore only the first core data are given here. The main sources of design data are refs. 2 and 3. The fuel in core 1 consists of slightly (1.5%) enriched UO_2. In table 2.a. the main data for core 1 are given. The cruciform control rods consist of 2% boron stainless steel alloy plates. However, after a short run these control rods were replaced by B_4C stainless steel rods. This change was not implemented in the present investigations.

The control rods enter from the bottom of the core. As cladding, channel and spacer material, Zircaloy-2 is used. In the DRESDEN 1 core 1 no burnable poison or curtains were used. In fig. 2.a. a horizontal section of a fuel assembly surrounded by light water and a quarter of a control rod is shown. In fig. 2.b. a horizontal section of a quarter of the core is shown. Fig. 2.c. shows a vertical section of the core.

The main data for a unit cell, dimensions and number densities at different temperatures are given in table 2.d. The pellet-to-clad gap was homogenized with the Zircaloy-2. In table 2.c. the control rod number densities are given.

The main hydraulic festures of the core are given in table 2.b. Each fuel element is surrounded by a zircaloy shroud and is thus considered a coolant channel. Different throttlings at the fuel channel inlets distribute the flow approximately proportional to the heat transfer load. At the top and bottom are support plates and along the channels three sets of spacers, all giving rise to singularities in the flow.

Since very few data have been available, the pressure drops across the different singularities have been adjusted to give the correct pressure drop across the core at the rated exit void and total mass flow.

Table 2.a.

DRESDEN 1 core 1 description

Core data	
Heat output (MW)	620
Net elect. (MW)	180
Active core height (cm)	275.4
Equivalent diameter (cm)	326
Fuel enrichment (w/o U^{235})	1.5
Number of fuel boxes max.	488
Number of rods in each box	36
Number of cruciform control rods	80
Fuel element pitch (cm)	12.85
Fuel rod pitch (cm)	1.8034
Fuel rod outside diameter (cm)	1.448
Fuel rod zircaloy-2 cladding thickness (cm)	0.0762
Fuel pellet diameter (cm)	1.255
Moderator temperature (°C)	284
Average clad temperature (°C)	294
Average fuel temperature (°C)	541
Average power density in core (W/cm^3)	31.2
Average power density (W/cm rod)	143.0
Connector length (cm)	4.45
Mass density UO_2 (g/cm^3)	10.44
Mass density zircaloy-2 (g/cm^3)	6.51
Mass density H_2O 20°C (g/cm^3)	0.9981
Mass density H_2O 284°C (g/cm^3)	0.7442
UO_2 linear expansion coefficient (10^{-5}/°C)	0.794
Zircaloy-2 linear expansion coefficient (10^{-5}/°C)	0.65

Table 2.b.

Core hydraulics data	
System pressure (bar)	69
Total mass flow rate (kg/s)	$4.764 \cdot 10^3$
Inlet subcooling (^oC)	21.8
Pressure drop across the core (bar)	0.53
Coolant channel flow area (cm^2)	61.50
Coolant channel hydraulic diam. (m)	0.1444
Moderator channel flow area (m^2)	1.691
Moderator channel hydraulic diam. (m)	0.02199
Shroud perimeter (m)	0.4420
Fuel pin perimeter per channel (m)	1.6174
Channel height (m)	2.7535

Table 2.c.

Control rod composition

Element	Weight percent (%)	Number density (10^{24} atoms/cm^3)
Fe	66.98	$5.6492 \cdot 10^{-2}$
Cr	16	$1.5805 \cdot 10^{-2}$
Ni	10	$0.8062 \cdot 10^{-2}$
C	0.02	$0.0356 \cdot 10^{-2}$
Mn	2.0	$0.1716 \cdot 10^{-2}$
Si	1.0	$0.1677 \cdot 10^{-2}$
B	2.0	$0.8713 \cdot 10^{-2}$

Density of control rod 7.95 g/cm^3

Table 2.d.

DRESDEN1 unit cell description

Region type	Cold	Doppler 1	Hot full power	Doppler 2
	Outer region radius (cm)			
Fuel (UO_2)	0.6274	0.6288	0.6300	0.6323
Clad (zircaloy-2)	0.7239	0.7252	0.7252	0.7252
Mod. (H_2O)	1.0175	1.0193	1.0193	1.0193
	Temperature (^oC)			
Fuel	20	300	541	1000
Clad	20	294	294	294
Mod.	20	284	284	284
	Number density (10^{24} atoms/cm^3)			
Fuel U^{235}	0.000354	0.000352	0.000350	0.000346
Fuel U^{238}	0.02295	0.02280	0.02266	0.02242
Fuel O	0.04661	0.04630	0.04604	0.04554
Clad Zr	0.0344	0.0342	0.0347	0.0355
Clad Fe	0.000073	0.0000731	0.000074	0.0000757
Mod. H, 0 per cent void	0.06680	0.04980	0.04980	0.04980
Mod. O, 0 per cent void	0.03340	0.02490	0.02490	0.02490
Mod. H, 25 per cent void		0.03736	0.03736	0.03736
Mod. O, 25 per cent void		0.01868	0.01868	0.01868
Mod. H, 50 per cent void		0.02490	0.02490	0.02490
Mod. O, 50 per cent void		0.01245	0.01245	0.01245

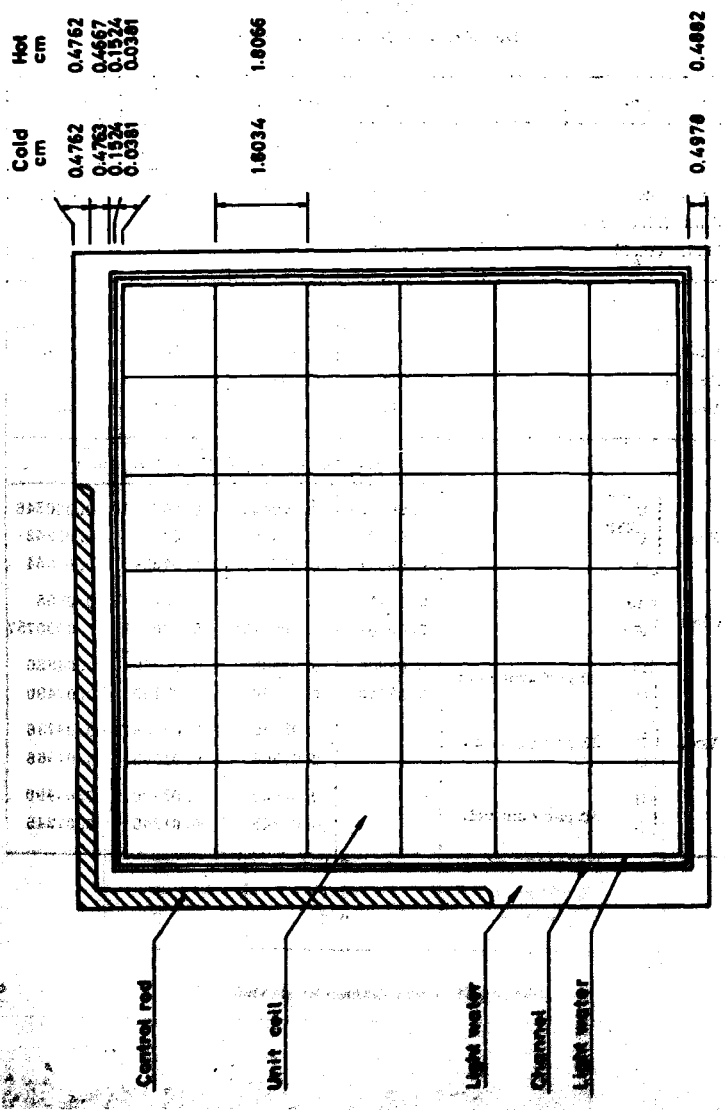

Fig. 2 a. DRESDEN 1 fuel box.

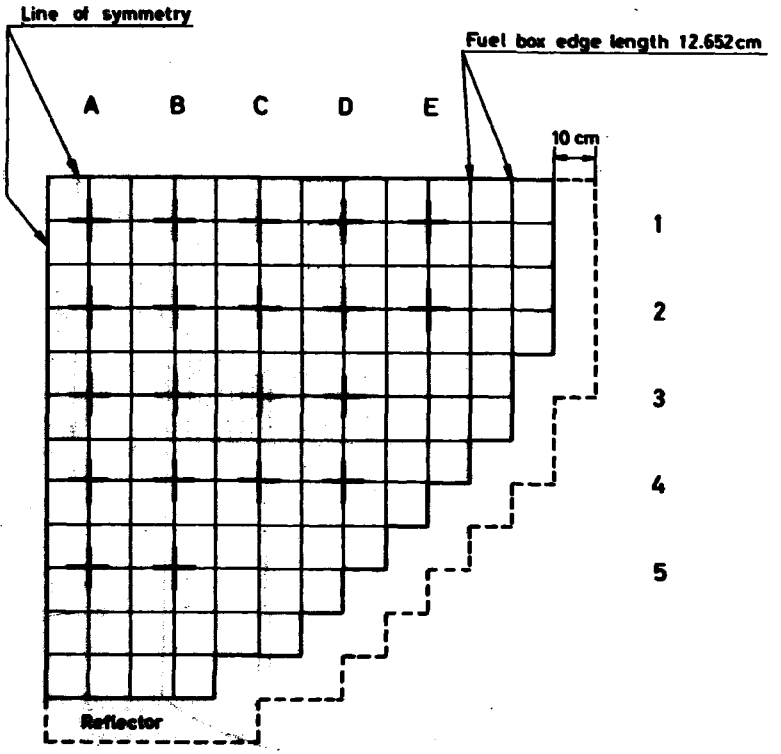

Fig. 2 b. DRESDEN 1 quarter core with dimensions and control rod identifications.

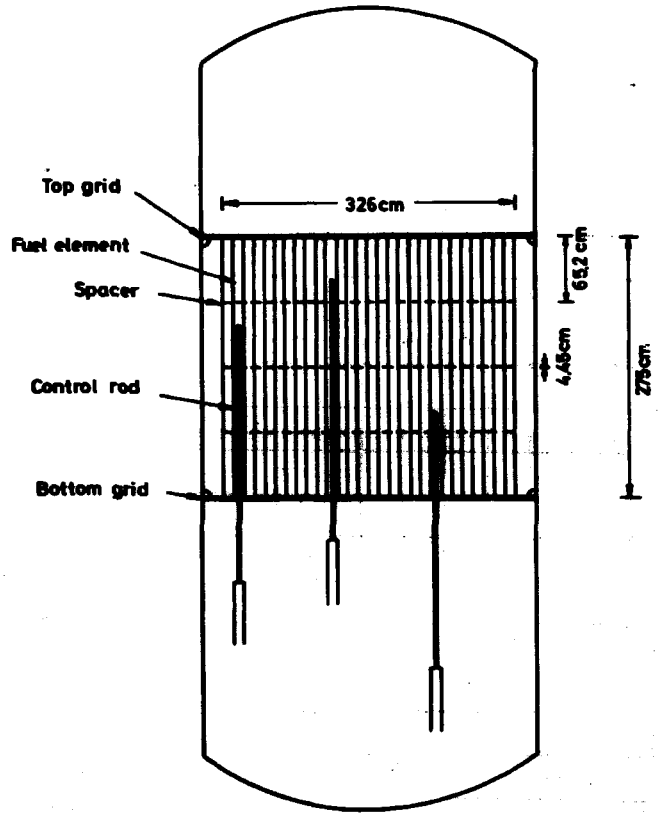

Fig. 2.c. Longitudinal section of the DRESDEN 1 reactor.

3. CROSS SECTIONS

The basis of the cross sections used in these calculations is the SIGMA MASTER TAPE[4] which contains 76-group cross sections generated from the UKNDL[5]. The MASTER TAPE cross sections must be supplied with thermal scattering data at the actual temperature and with shielded resonance cross sections. This is done by the program CRS[6], which can then do a spectrum calculation, collapse the cross sections into fewer groups and edit the collapsed cross sections in formats suitable for the next stage of computer codes.

For the generation of thermal scattering cross sections, the present version of CRS contains a routine NELKINSCM[7]. NELKINSCM calculates group transfer cross sections from the Nelkin model for H bound in H_2O and from the similar model for D. For all other materials the free gas model is used. For U^{238}, U^{235} and Pu^{239} in the resonance region group constants may be calculated by the RESAB PROGRAMME SYSTEM[8, 9] or in CRS itself by the routine RESOREX[10], which utilizes tabulations from RESAB by means of an equivalence principle. For all other resonant materials the infinite dilute cross sections from the MASTER TAPE are kept unaltered. In all the DRESDEN calculations of this report RESOREX is used for the resonance treatment.

For burn-up calculations a special library of fission product data, the FIPO library[11], is used. It contains yields, decay constants and absorption cross sections for 166 different fission products from the three nuclides U^{235}, U^{238}, Pu^{239}. The absorption cross sections for some of the fission products originate in the UKNDL and are given in 10 groups, for other nuclides only a thermal cross section or a resonance integral or both are found in the library.

3.1. Energy Group Structures

In tables 3.1.a. and 3.1.b. the energy boundaries of the group structures applied in the different types of calculations are shown. The 10-, 5- and 2-group structures are subsystems of the original 76-group structure and they are used subsequently in the calculations so that more and more detailed spatial representations are made possible by reductions in the energy solution.

The 76 groups of the MASTER TAPE are divided into 41 fast and 35 thermal groups, which means that the calculation of thermal transfer ma-

Table 3.1.a.

Energy group structures. Fast part.

76 groups		10 groups		5 groups		2 groups	
Group No.	Upper energy boundary (MeV)	Group No.	Upper energy boundary (MeV)	Group No.	Upper energy boundary (MeV)	Group No.	Upper energy boundary (MeV)
1	15	1	15	1	15	1	15
2	10						
3	7.7880						
4	6.0653						
5	4.7237						
6	3.6788						
7	2.8650						
8	2.2313						
9	1.7377						
10	1.3533						
11	1.0540						
12	8.2085×10^{-1}						
13	6.3928×10^{-1}						
14	4.9787×10^{-1}	2	4.9787×10^{-1}	2	4.9787×10^{-1}		
15	3.8774×10^{-1}						
16	3.0197×10^{-1}						
17	2.3518×10^{-1}						
18	1.8316×10^{-1}						
19	1.4264×10^{-1}						
20	1.1109×10^{-1}						
21	8.6517×10^{-2}						
22	6.7379×10^{-2}						
23	5.2475×10^{-2}						
24	4.0868×10^{-2}						
25	3.1828×10^{-2}						
26	2.4788×10^{-2}						
27	1.9305×10^{-2}	3	1.9305×10^{-2}	3	1.9305×10^{-2}		
28	1.5034×10^{-2}						
29	1.1709×10^{-2}						
30	9.1188×10^{-3}						
31	7.1017×10^{-3}	4	7.1017×10^{-3}				
32	5.5308×10^{-3}						
33	4.3074×10^{-3}						
34	3.3546×10^{-3}						
35	2.6126×10^{-3}						
36	2.0347×10^{-3}						
37	1.5846×10^{-3}						
38	1.2341×10^{-3}						
39	9.6112×10^{-4}						
40	7.4852×10^{-4}						
41	5.8295×10^{-4}						

Table 3.1.b.

Energy group structures. Thermal part.

76 groups		10 groups		5 groups		2 groups	
Group No.	Upper energy boundary (MeV)	Group No.	Upper energy boundary (MeV)	Group No.	Upper energy boundary (MeV)	Group No.	Upper energy boundary (MeV)
42	1.0130×10^{-6}	5	1.0130×10^{-6}	4	1.0130×10^{-6}	2	1.0130×10^{-6}
43	1.7262×10^{-6}						
44	1.5060×10^{-6}						
45	1.4875×10^{-6}						
46	1.3879×10^{-6}						
47	1.1884×10^{-6}						
48	1.0007×10^{-6}	6	1.0007×10^{-6}				
49	1.0722×10^{-6}						
50	1.0634×10^{-6}						
51	1.0525×10^{-6}						
52	1.0430×10^{-6}						
53	1.0137×10^{-6}	7	1.0137×10^{-6}				
54	9.5070×10^{-7}						
55	7.8211×10^{-7}						
56	9.3488×10^{-7}	8	6.3488×10^{-7}	5	6.3488×10^{-7}		
57	5.0338×10^{-7}						
58	4.1704×10^{-7}						
59	3.5768×10^{-7}						
60	3.2064×10^{-7}						
61	3.0113×10^{-7}						
62	2.9076×10^{-7}						
63	2.7833×10^{-7}						
64	2.5106×10^{-7}	9	2.5106×10^{-7}				
65	2.2770×10^{-7}						
66	1.9064×10^{-7}						
67	1.4572×10^{-7}						
68	1.1157×10^{-7}						
69	8.1572×10^{-8}						
70	5.8295×10^{-8}						
71	4.2757×10^{-8}	10	4.2757×10^{-8}				
72	3.0119×10^{-8}						
73	2.0893×10^{-8}						
74	1.2907×10^{-8}						
75	6.3928×10^{-9}						
76	3.9790×10^{-9}						

trices is limited to the 35 lowest energy groups. Thermal cutoff is thereby defined to be 1.855 eV and upscattering above this limit is neglected. Shielded resonance cross sections are introduced for U^{238} in the 22 and for U^{235} and Pu^{239} in the 14 groups just above the thermal limit so that the resonance region of U^{238} is 1.855 eV - 111.09 keV and that of the two fissile isotopes is 1.855 eV - 3.3546 keV.

For burn-up calculations at the pin cell level, the 10-group subsystem is used. It consists of 4 fast and 6 thermal energy groups. One of the thermal groups, group no. 6, is very narrow and is situated round the Pu^{240} resonance at 1.056 eV. The 5-group, 3 fast and 2 thermal groups, system is used for two-dimensional calculations of the box flux-distribution. Overall calculations in three dimensions are performed in only 2 energy groups.

The 10-, 5-, and 2-group systems have previously been applied to calculations on the Yankee PWR reactor as described in ref. 1.

3.2. 10-group Cross Sections for Burn-up Calculations

The generation of a 10-group set of microscopic cross sections for the burn-up codes CEB and CDB[1] is shown in the block-diagram fig. 3.2.a. CDB is the burn-up program employed for the calculations on the DRESDEN 1 fuel box; it combines collision probability theory on pin cells and diffusion theory for the box flux-solution. The fast unit cell burn-up program CEB is used for investigations previous to the CDB calculations. Both codes need microscopic nuclear data with the same format.

A 10-group data set refers to a given unit cell for which the geometric data, isotopic compositions and temperatures in fuel, clad and moderator must be specified. For the condensation from 76 into 10 groups a homogeneous spectrum is calculated. The three regions of the unit cell are smeared out, and the 0-dimensional flux spectrum is calculated in 76 groups for the resulting mixture with an imposed overall buckling.

The homogenization before the spectrum calculation is of course an approximation, which limits the degree of group collapsing, especially in the thermal region where the flux depression in the fuel is most important. It is hoped that the 6 thermal groups of the 10-group system give a sufficiently good energy solution so that too severe errors are not introduced at the condensation. For a boiling water reactor like DRESDEN 1 not even a unit cell spectrum calculation is satisfactory, because it ignores the influence from the broad water gaps between the boxes, and as no available

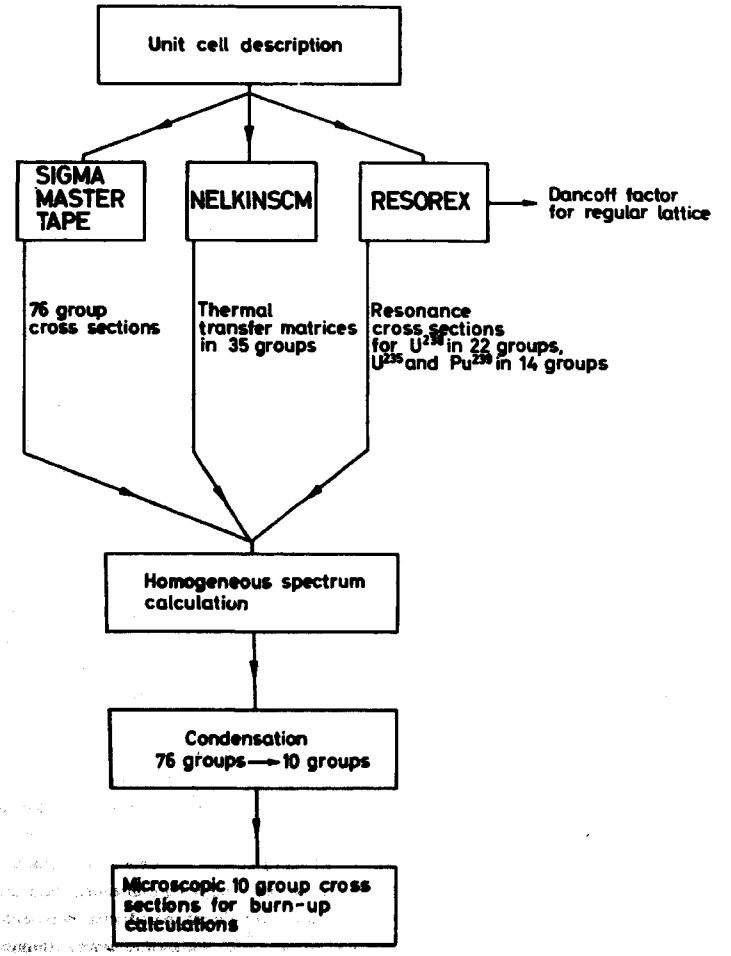

Fig. 3.2.a. Generation of microscopic cross sections for burn-up calculations.

program is able to handle this effect properly, the simplest possible spectrum calculation was chosen.

Two sets of resonance cross sections are produced by the routine RESOREX: One set averaged for the fuel and one averaged for the whole cell. The cell averaged set is used for the homogeneous spectrum calculation, but is replaced by the fuel averaged set before the condensation, because the subsequent calculations are collision probability theory in three regions with the fuel as one of them.

As it seems that the RESAB - RESOREX resonance treatment overpredicts the U^{238} resonance integral, a correction to the resonance group cross section is introduced. The correction is that proposed by Fayers et al. in ref. 12:

$$\frac{\Delta I^g}{\tau} = 0.2 \times \left(1 - \frac{3}{2}\frac{I^g}{\sigma_p \tau}\right) \text{ barn.}$$

I^g is the group resonance integral, τ the lethargy width of the group and σ_p is the effective NR-scattering cross section per U^{238} atom[10]. This correcting term is subtracted from the shielded cross sections of U^{238} in the groups 28-41 of the 76-group system corresponding to the energy region 1.855 eV - 3.3546 keV, by which the total resonance integral is reduced by about 10%.

Besides the effective resonance cross sections, RESOREX gives the Dancoff factor to be used later in the box calculation. In fact two different Dancoff factors are calculated, a narrow resonance and a wide resonance Dancoff factor, with different treatments of the cladding region. The correct Dancoff factor should lie somewhere between the two values. Fortunately the difference between them is small, and in the present calculations the narrow resonance Dancoff factor has been chosen.

In the burn-up codes CEB and CDB[1], the heavy nuclide chains of U^{235} and U^{238} are treated so that the U^{235} chain is terminated after U^{236} and the last isotope in the U^{238}-Pu system is Pu^{242}. In the UKNDL, and consequently on the SIGMA MASTER TAPE, the cross sections of U^{236} are incomplete (only given for energies > 1 keV) and Pu^{242} cross sections are completely missing. Nothing has been done to supply the missing data from other sources, so the burn-up calculations were performed with zero cross sections for U^{236} at low energies and for Pu^{242}. This of course influences the build-up of the two isotopes in question, but as neither is very important at moderate burn-up values because of their relatively low absorption cross

sections and the low concentration of Pu^{242}, this lack is supposed to be unimportant for the rest of the burn-up calculation.

3.3. 5- and 2-group Cross Sections for Non-burnable Regions

Besides the unit cell microscopic data in 10 groups, macroscopic cross sections are needed for the zircaloy channel round the fuel box, the water filling the gaps between the boxes and the water reflector surrounding the core. All of these materials are situated outside unit cell regions and consequently their flux spectrum differs from that used for generating the cell cross sections. Furthermore, the cross sections for non-burnable regions must be given in the few-group structures applied in the box and overall flux calculations, i.e. 5 and 2 groups, which stresses the need for a good spectrum determination for the regions in question. A homogenization corresponding to the unit cell treatment is therefore not adequate.

In the block-diagram fig. 3.3.a. the calculation flow is shown for a few-group macroscopic cross section generation. At first macroscopic cross sections for the non-burnable material compositions in the 76-group MASTER TAPE structure are produced together with a set of 76-group macroscopic cross sections for a homogenized unit cell, which in fact is the same cross section set as the one used for the homogeneous spectrum calculation of section 3.2. These data are fed into the one-dimensional collision probability theory program GP[13], which is able to do a flux calculation in 76 groups. The non-burnable material cross sections are then collapsed into few groups with the fluxes found in the corresponding regions. The specific composition of the homogenized fuel-moderator region is not considered to be very important as it is only used as a "driver zone" in the flux calculation, and therefore a standard fuel mixture (isotopic composition corresponding to a burn-up of about 1000 MWD/TU, mean void = 25% and temperatures as for hot, full power conditions) is applied in all calculations.

For the CDB box calculations, cross sections in the 5-group structure for the water gap between the boxes and the zircaloy-2 channel round the fuel element are needed. (The generation of cross sections for control rods is described in chapter 6). Figs. 3.3.b. and 3.3.c. show the channel and gap dimensions for the two cases with and without a control rod position. A fuel element in the interior core has the broad gap at two adjacent sides and the narrow one at the other two. In the water gap between the boxes no boiling occurs, but in the very narrow water gaps between the channel and the unit cell region the void content is varying together with that of the fuel

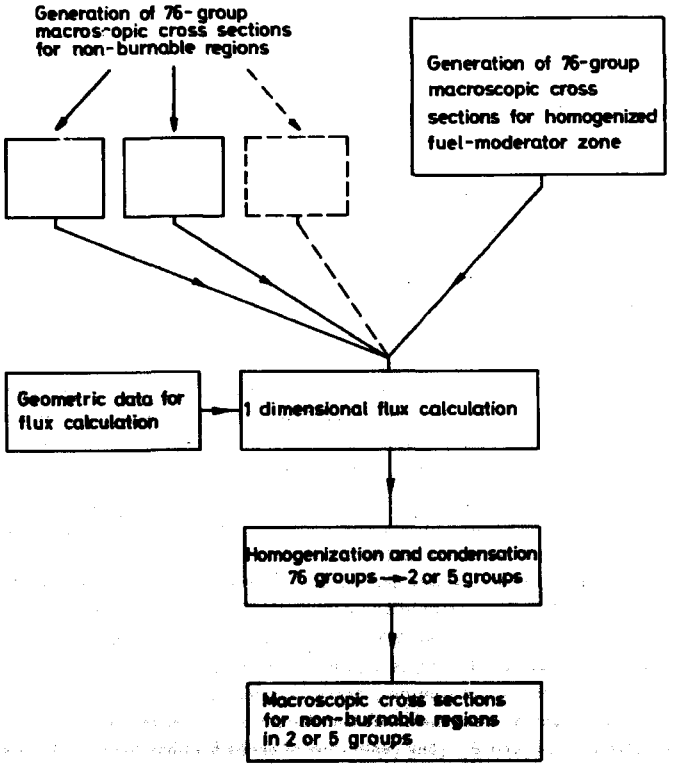

Fig. 3.3.a. Generation of macroscopic few-group cross sections for non-burnable regions.

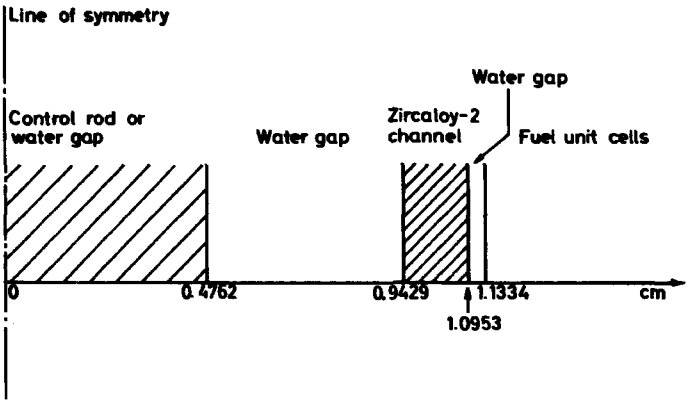

Fig. 3.3.b. Fuel box gap at control rod position. Hot dimensions.

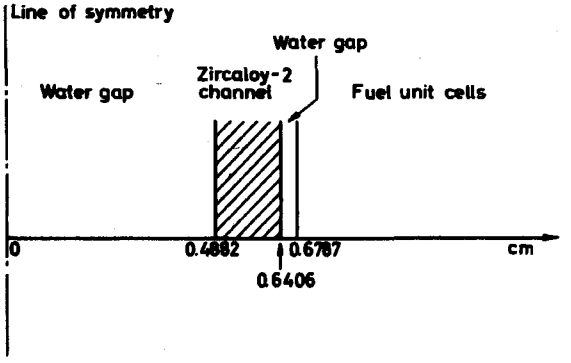

Fig. 3.3.c. Fuel box gap without control. Hot dimensions.

element. In principle the few-group cross sections of channel and water gaps are therefore dependent both upon the height in the reactor core and upon which side of the box is referred to; for practical reasons, however, it was decided to generate only one set of "mean" cross sections.

In fig. 3.3.d. the set-up of the GP-calculation is shown. The width of the water gap is taken as the mean value between the broad and the narrow ones. Of regard for the difference equation technique used in CDB the zircaloy channel is combined with the narrow water gap inside the box and some of the water from the inter-box gap, to form a homogenized material zone which can be used as one mesh in CDB. The void content inside the channel was chosen to be 25%. Of the zircaloy components only Zr and Fe were accounted for. The most important alloying component, Sn, is not included in the data library and the zircaloy-2 in the calculations is therefore Zr containing 0.13% Fe. The mesh division and boundary conditions for the collision probability calculation appear from fig. 3.3.d. The compositions 1 and 2 are collapsed into 5 groups for CDB.

2-group cross sections for the reflector water to be used in overall calculations are generated by a similar slab geometry calculation. The transition from core to reflector is sketched in fig. 3.3.e. beginning from the middle of the edge fuel box. The reflector water has on the average a thickness of about 10 cm. In fig. 3.3.f. is shown the collision probability theory calculation which produces the reflector spectrum. A symmetry line is placed in the middle of the fuel box, the box channel is represented by the same zircaloy-water mixture as in the inter-box calculations and a black boundary is assumed after 10 cm of reflecting water. The water, composition no. 3, is condensed into 2 groups after the spectrum calculation. This is done with 0-void water to be used at the bottom of and beside the core and with water containing 50% void for the top reflector.

For use in calculations on initial criticality the whole procedure for non-burnable materials was repeated, the only differences being that cold dimensions and room temperature were used together with isotopic composition in fuel mixture corresponding to cold clean condition with no void in the coolant.

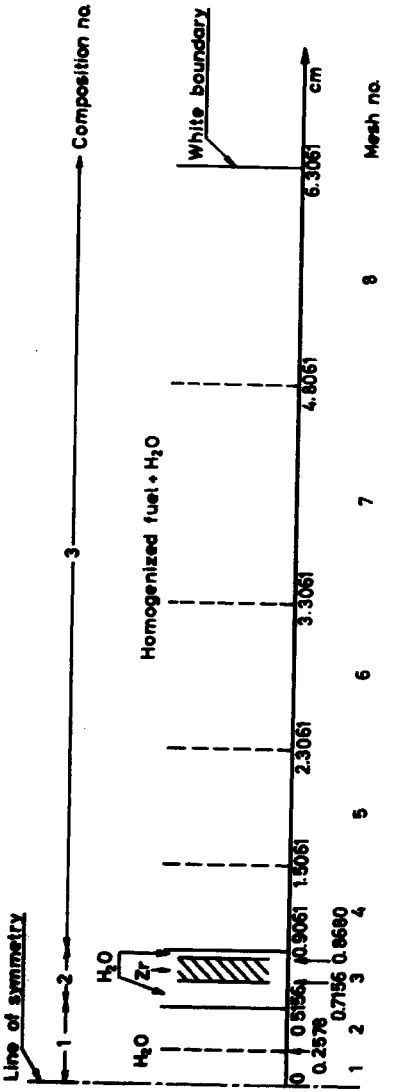

Fig. 3.3.d. Material compositions and mesh division for GP slab geometry calculation of few-group macroscopic cross sections for fuel box gap.

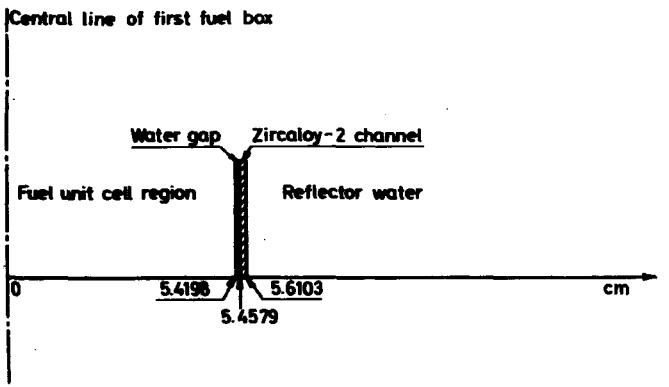

Fig. 3.3.e. Fuel region-reflector boundary. Hot dimensions.

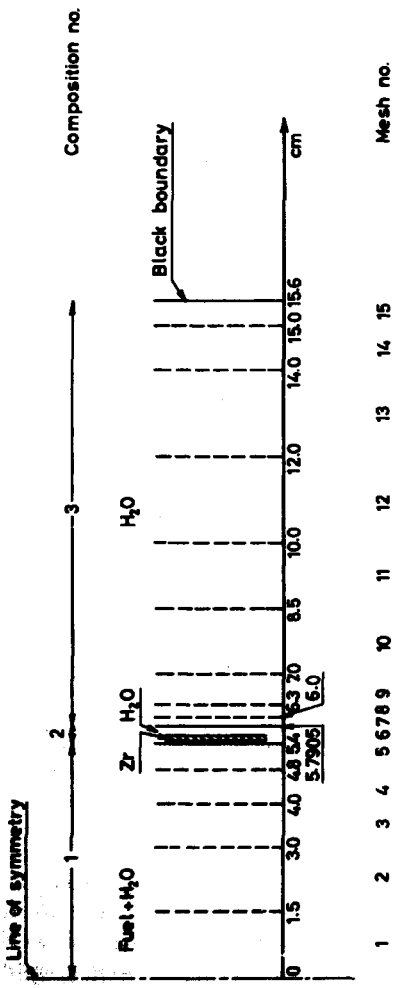

Fig. 3.3.f. Material compositions and mesh division for GP slab geometry calculation of few-group macroscopic cross sections for reflector.

4. UNIT CELL BURN-UP INVESTIGATIONS

Because of the small number of fuel rods in a BWR-element (in the case of DRESDEN 1 6x6) and the influence from the broad water gaps, no asymptotic unit cell exists; in fact the smallest unit in the core treatment is the fuel box surrounded by the water belonging to it. A box burn-up calculation is, however, a time-consuming matter, and therefore a number of unit cell burn-up calculations were carried out prior to the elaborate box calculations to check the significance of a more or less refined data supply, the time-step length, etc. The unit cell burn-up code used for these investigations is CEB[1], which is also the cell burn-up code incorporated in the box program CDB.

The CEB program is a collision probability theory code which calculates the flux in the regions asked for at the beginning of each time step and assumes the flux distribution to be constant during the step (quasi-stationary approach). Common to all unit cell calculations described here is that they are burn-up calculations in cylinder geometry for a fuel rod surrounded by moderating light water with white surface as boundary condition. The calculations are performed in three regions: fuel, clad and moderator, and with only one mesh in each region. The cross sections applied are 10-group microscopic cross sections generated as described in section 3.2.

4.1. Description of Unit Cell Calculations

All burn-up calculations at the unit cell and box level have to be performed in 10 groups partly in regard to computing time and partly because of the fission product library, which is given in the 10-group structure. But if the cross sections are collapsed from 76 to 10 groups at the start of the calculation, i.e. at clean conditions, the influence of burn-up on the fine group spectrum will be ignored. Furthermore, as demonstrated in ref. 10, the group cross sections for Pu^{239} generated by the routine RESOREX are inaccurate for mixtures with very low concentrations of the isotope. To find out the importance of these effects, unit cell burn-up calculations were performed with frequent regeneration of the 10-group cross section set as the change in fuel isotopic composition proceeded.

In fig. 4.1.a. the calculated Pu build-up is shown for a unit cell containing 35% void in the moderating water and with the detailed fission product treatment of the FIPO-routine. The cross sections were regenerated twice, at 1035 MWD/TU and at 4712 MWD/TU. For comparison the concentrations

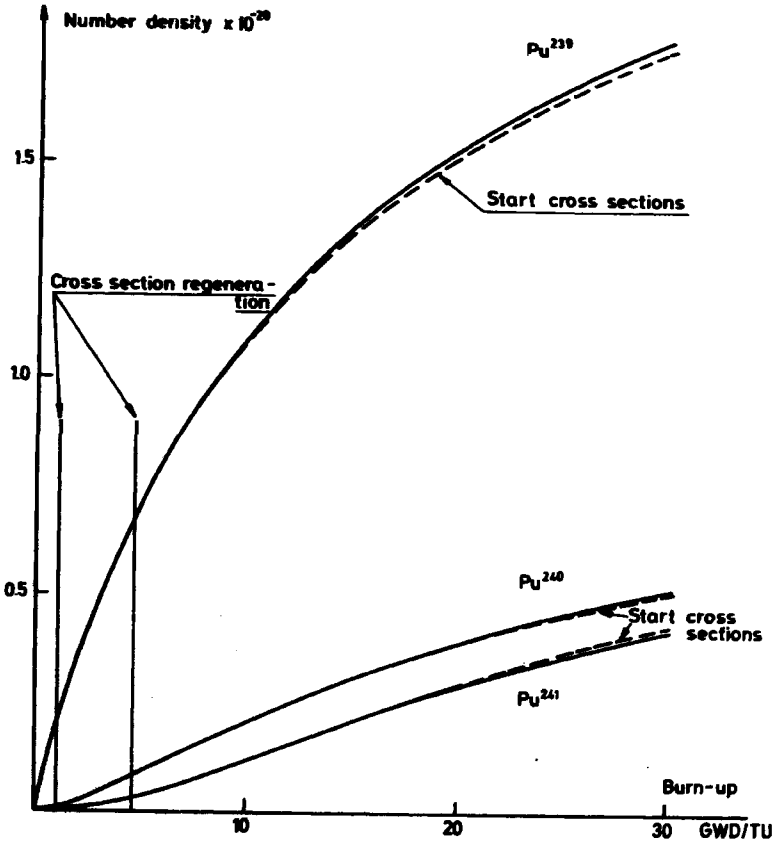

Fig. 4.1.a. Pu build-up with and without regeneration of the 10-group data set. Unit cell calculations.

obtained by using the clean condition cross sections are shown with dotted lines. It is seen from the figure that the effect of fine group spectrum recalculation is of minor importance for the burn-up of this type of fuel cell. The effect on k_{eff} was correspondingly small. Calculations for other void fractions showed a similar small influence from the recalculations, and for the following unit cell investigations it was therefore decided to use only one set of microscopic 10-group cross sections all through the burn-up. This cross section set was in all cases generated for the isotopic composition found at 1035 MWD/TU.

The demonstrated insensibility of the 10-group cross sections to fine group spectrum recalculations is a very fortunate thing for the present calculations, as it is almost impossible to regenerate cross sections during burn-up for the different pins in a fuel box, but it cannot be expected to be valid in general. Especially in fuel cells where burnable poisons, for instance Gd, are present, the fine group spectrum and therefore also the 10-group cross sections may be strongly dependent on burn-up.

One place where computer time saving approximations is relevant is in the calculation of fission product poisoning. In a unit cell calculation with the program CEB[1], it is possible to use the detailed fission product burn-up by using the FIPO routine[11]. But in fact when CEB-FIPO is used most of the computer time used is spent in the FIPO-calculation, so in the more expensive box calculation with the program CDB[1] there is much time to save by avoiding the use of FIPO. This is most easily done by taking the fission product poisoning in 10 groups as calculated by FIPO at a selected burn-up stage in the unit cell calculation and from this generate a 10-group fission product cross section per fission, which is then used instead of FIPO. To check how serious errors are introduced by this procedure a series of unit cell calculations was performed with fission product cross sections taken at different burn-up values for comparison with the detailed FIPO-treatment.

In figs. 4.1.b. and 4.1.c. the results of such calculations are drawn. The pin cell is again a DRESDEN 1.5% enriched unit cell with a void content of 25%, which is about mean void for the reactor. The FIPO-calculation is compared with two approximate calculations - one having a fission product cross section taken at 4712 MWD/TU and the other with a fission product from 12884 MWD/TU. The influence on the build-up of Pu is rather small as seen from fig. 4.1.b., in the cases of Pu^{240} and Pu^{241} the different curves may not even be distinguished. On the other hand the errors in k_{eff} is very important, except for the burn-up values close to where the fission

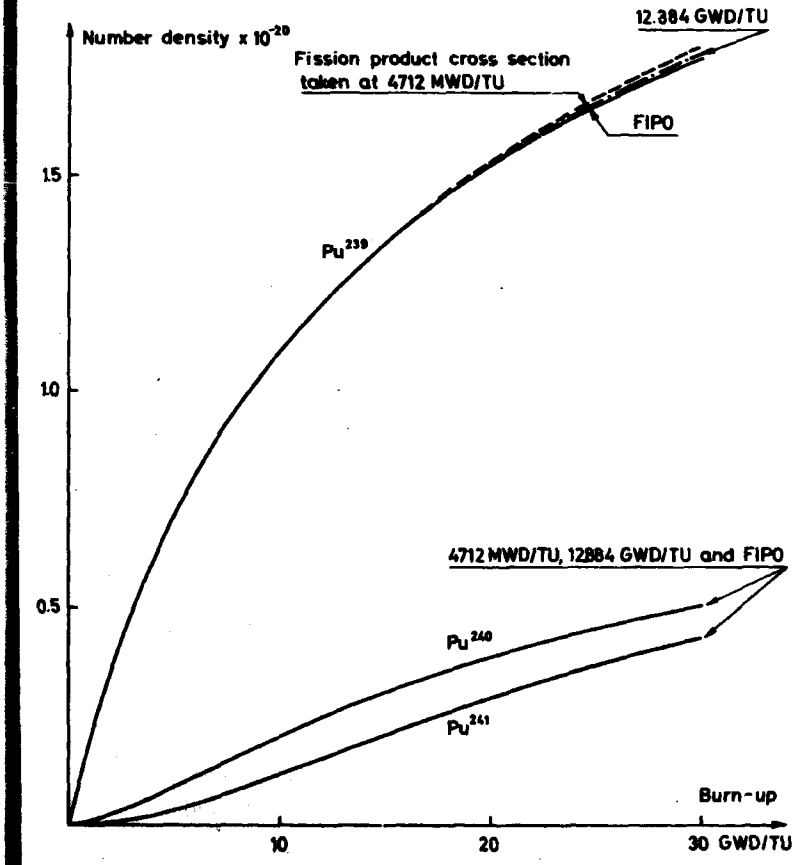

Fig. 4.1.b. Pu build-up with different fission product treatments. Unit cell calculations. 25% void.

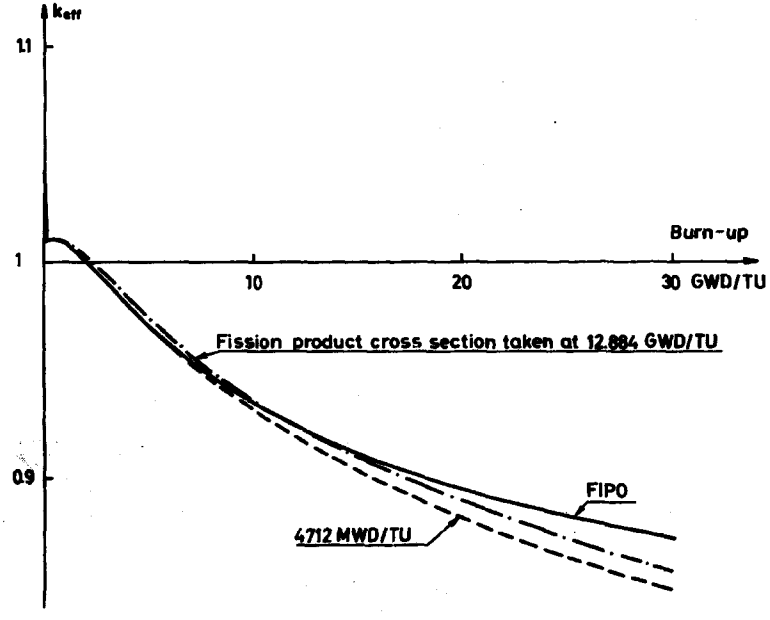

Fig. 4.1.c. k_{eff} versus burn-up with different fission product treatments. Unit cell calculations. 25% void.

product cross section was generated. This indicates that although the magnitude of the fission product poisoning is wrong (error in k_{eff}), the spectrum calculation must be rather unspoiled by the approximation to give the good agreement in isotopic compositions.

The influence of the moderator void content on the build-up of Pu^{239} is shown in fig. 4.1.d. for 0%, 25% and 50% void, and the corresponding k_{eff} curves are given in fig. 4.1.e. The very great differences in the Pu-concentration show that it is important to be able to calculate the actual void content accurately in order to predict the isotopic compositions during burn-up. From fig. 4.1.e. it is seen that the increasing Pu-production for higher void contents gives a slower fall in k_{eff}. A similar variation in the burn-up picture may be obtained by adding more water round the unit cell without varying the water density. The rather low values of k_{eff} suggesting that the reactor might fail to get critical are only due to the fact that the calculations were performed for asymptotic unit cells without regard to the great influence from the water gaps surrounding the fuel box.

In order to ascertain if the dependence of the 10-group microscopic cross sections on the void content is small enough to allow the use of only one set of 10-group cross sections for all voids, the calculations for 50% void were repeated, but with the cross sections generated for the 0% void case. The result is shown as the dotted lines on the figs. 4.1.d. and 4.1.e. The influence of water density on the 10-group cross sections does not seem to be negligible.

Finally a series of unit cell burn-up calculations was run to examine the significance of the time step length. Twice as long time steps mean nearly halving of computing time and consequently it is important to know exactly, with a view to time-consuming burn-up calculations, at which length of the burn-up steps serious errors begin to arise. In figs. 4.1.f. and 4.1.g. the results of such calculations are shown. The shortest time step, 60 days, corresponding to 800 MWD/TU, is small enough to be taken as a reference since shorter steps do not practically make any difference. The curves for a step length of 180 days are shown for comparison. A calculation with a 120-day step length gave results lying half-way between the two curves. In all cases the burn-up was started by two steps of 4 and 12 days to account for Xe and Sm build-up and thereafter three 30-day steps to give the form of the small bump at the beginning of the k_{eff}-curve.

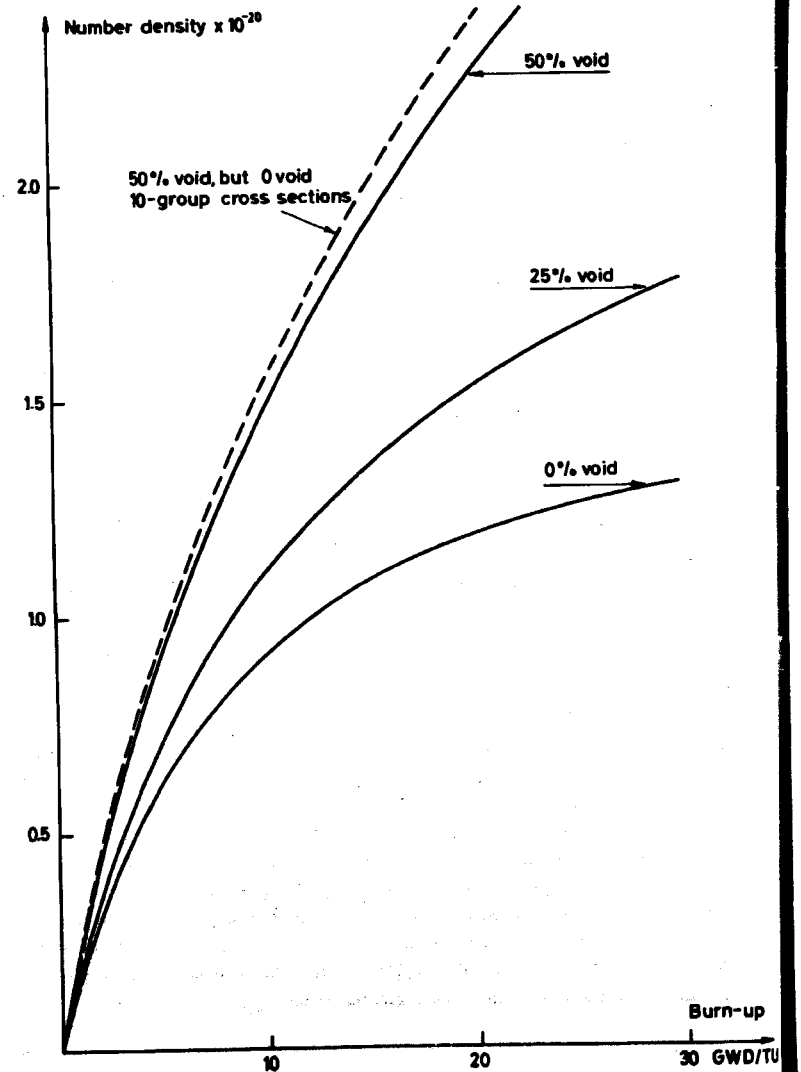

Fig. 4.1.d. Production of Pu^{239} for different void fractions. Unit cell calculations.

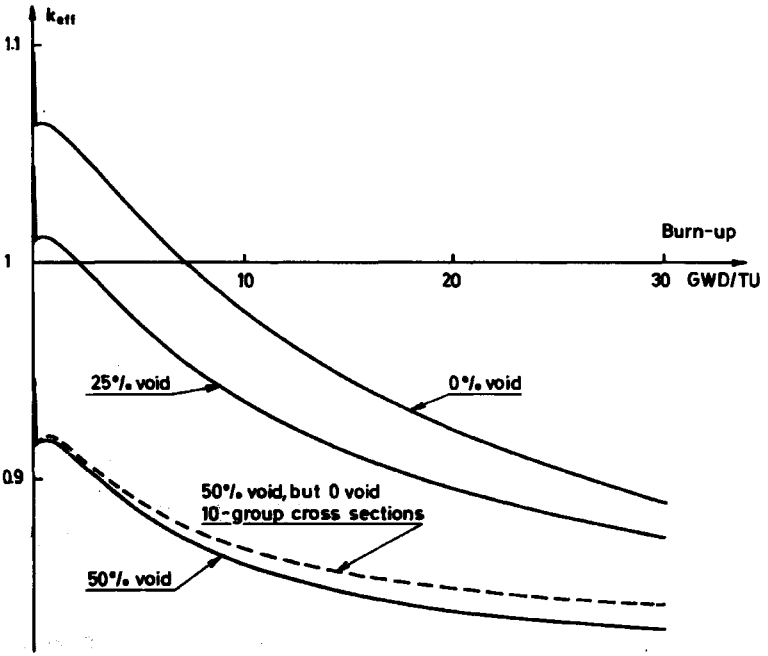

Fig. 4.1.e. k_{eff} as a function of burn-up for different void fractions. Unit cell calculations.

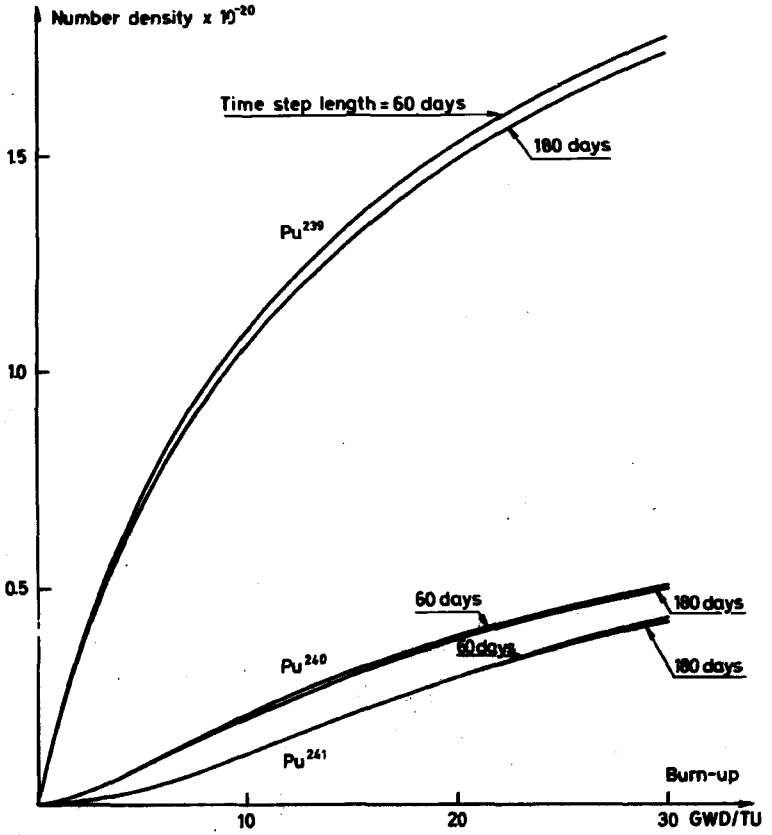

Fig. 4.1.f. Pu build-up for different time step lengths. Unit cell calculations. 25% void.

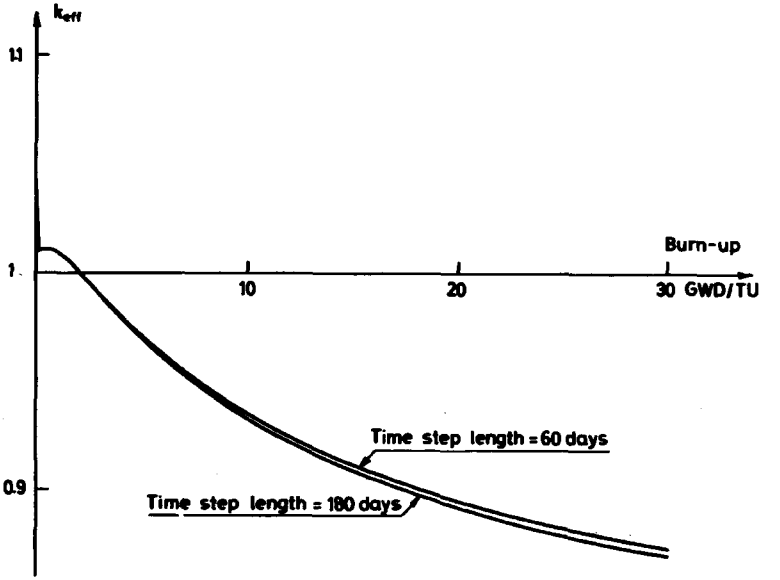

Fig. 4.1.g. k_{eff} versus burn-up as a function of time step length. Unit cell calculations. 25% void.

4.2. Strategy in Unit Cell Data Supply for Box-calculations

As a conclusion to the unit cell burn-up investigations the following microscopic 10-group cross section treatment was decided upon for the box burn-up calculations:

1) One set of 10-group microscopic cross sections was used for all values of burn-up from 0 to 30000 MWD/TU. This cross section set was chosen to be the one generated for the isotopic composition taken from an asymptotic unit cell calculation at 1035 MWD/TU. The errors introduced by this approximation, i. e. a few per cent too low Pu-production at very high burn-up values, are thought to be insignificant compared to the prohibitive amount of work needed to regenerate cross sections during burn-up.

2) In one single case a box burn-up calculation was carried out with the detailed FIPO fission product treatment to serve as a reference, but for all other calculations a fixed 10-group cross section per fission had to be used. Out of the results of the unit cell calculations the fission product cross section taken at 12884 MWD/TU was chosen. This is not expected to introduce errors in isotopic composition at reasonable burn-up values; as to the value of k_{eff} which is becoming far too low from about 15000 MWD/TU, it is interesting only in the three-dimensional overall calculations, and these will only be carried out for the first fuel cycle, i. e. until a mean exposure of about 6000 MWD/TU.

3) It was decided to do the box calculations for three different void contents, 0%, 25% and 50% void, corresponding approximately to the bottom, the middle and the top of the core. From the experience with unit cells it was concluded that the microscopic 10-group cross section had to be generated for the actual void content, which means that three sets of microscopic 10-group data, for 0%, 25% and 50% void, are necessary.

4) The time step length for the box burn-up calculations was chosen to be 120 days after the initial short steps, because the 180-step curves drawn in figs. 4.1.f. and 4.1.g. were found to deviate a little too much from the 60-day calculations. The burn-up steps of 120 days will give a build-up of Pu which is a bit too low, but not more than tolerable, the saving in computer time taken into consideration. The time steps from the clean box start will then be 4, 12, 30, 30, 30 and 120 days during the rest of the burn-up.

All condensing of microscopic cross sections from 76 into 10 groups was performed with a spectrum calculated by assuming a buckling corresponding to the reactor overall buckling in all energy groups. This buckling was shown to have only a very small influence on the calculated spectrum, and it is therefore quite unimportant for the 10-group cross sections too.

Finally it should be pointed out that all microscopic 10-group cross sections have been generated for an asymptotic unit cell, i. e. a fuel pin surrounded by the water belonging to it according to the pitch, but without regard to the influence form the water gaps between the boxes. Perhaps a better approach would have been to define a sort of equivalent cell containing a proper amount of additional water. No investigations of this kind have been carried out.

5. FUEL BOX CALCULATIONS

For the depletion calculations on fuel assemblies the fuel box burn-up code CDB, described in ref. 1, was used. This program combines the unit cell depletion calculation and a two-dimensional diffusion theory flux solution for the fuel element with its surrounding water-gaps.

The box calculations performed are intended to serve two, in principle different, purposes:

1) The calculated isotopic compositions and reactivity values as function of burn-up may be compared first of all with available measurements, but also with box burn-up calculations published from other places. Such comparisons form to a certain degree a control of the calculations until this point.

2) By homogenization of the fuel box at intervals during the burn-up, cross sections are produced for use in the subsequent three-dimensional overall burn-up calculations. The box calculations for this purpose are described in chapter 9.

It seems that only few depletion measurements have been published for boiling water reactors. For the DRESDEN 1, however, some isotopic composition data from the end of the first fuel cycle are found in ref. 14. In ref. 15 measured isotopic compositions have been reported for exposure values until 20000 MWD/TU. Besides these measurements, the calculations of ref. 16 will be used for comparisons; they are box burn-up calculations in the ISOCHECK series carried out by Combustion Engineering for the USAEC.

5.1. Description of the Box Calculations

The program CDB for box depletion calculations must be supplied with two sorts of cross sections: microscopic unit cell data for the burn-up of the individual fuel pins and macroscopic cross sections for non-burnable regions. The microscopic data sets are selected on the basis of unit cell calculations as described in chapter 4 and generated by the methods of section 3.2. All unit cell depletion calculations are performed in the 10-energy-group structure. For the box flux-solution the 5-group structure was used, and hence the macroscopic cross sections were generated in 5 groups by the procedures described in section 3.3. No control rod data are needed for the calculations of this chapter as fuel boxes here are only depleted in the control-rod-out condition. The reason for this simplification was that no information is given concerning the control rod movements in the neighbourhood of the measuring points; it is only said that the fuel assemblies from which the experimental samples were taken were chosen sc that most of the time in the core they had been operated with the adjacent control rods withdrawn.

The mean outlet void content is about 47% for the DRESDEN 1 reactor. In ref. 15 measurements are given for different axial positions from the no void condition at the bottom of the core to the maximal void at the top. The calculations in ref. 16 were performed with 0%, 25% and 50% void. It was therefore decided to carry out box depletion calculations for the three values 0%, 25%, and 50% of void to allow direct comparison with the calculations of ref. 16, at the same time achieving good comparability to the experiments.

The DRESDEN 1 fuel element with its 6x6 fuel rods surrounded by shroud and water gap is shown in fig. 2.a. in chapter 2. The mesh division for the box burn-up calculations can be seen from fig. 5.1.a. The numbers in the figure are the composition numbers in the calculations and their meaning is as follows:

Composition no. 1: white boundaries
" " 2: water
" " 3: homogenized water and zircaloy as described in section 3.3.

Composition nos. 2-3 represent non-burnable regions and their cross sections are therefore not changed during the burn-up.

The burnable regions are given the composition numbers 4 - 9. Fuel pins having the same composition number are treated as identical - in other words the box calculations are performed as if only 6 different isotopic com-

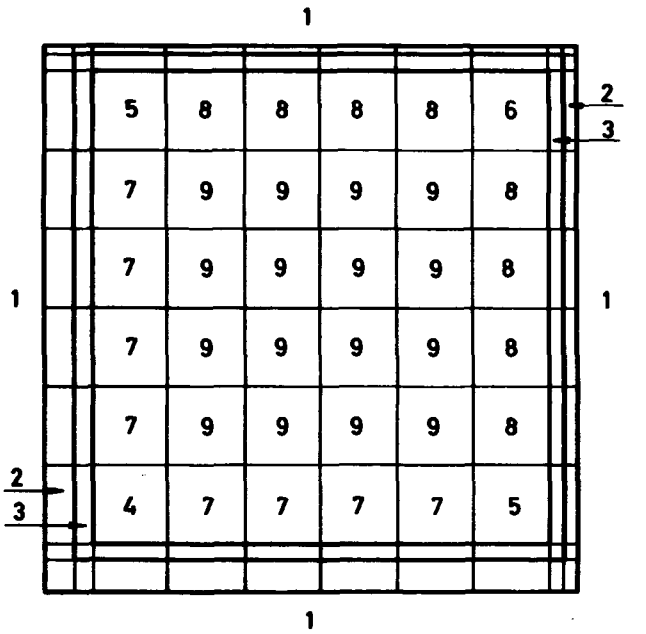

Fig.5.1.a. Composition numbers and mesh division for box depletion calculations.

positions of fuel were present. Test runs were made with more detailed description, but the difference in calculated isotopic compositions was very small whereas computing time increases rapidly with the number of fuel pins individually accounted for.

The resonance shielding for fuel rods at different places in the assembly is taken into account in CDB by means of the Dancoff correction

$$DC = \sqrt{\frac{1 - gC}{1 - C}},$$

which must be specified as input for each type of fuel pin. The value of 1-C is obtained from the generation of microscopic cross sections; it is the Dancoff factor for the asymptotic fuel rod which is calculated by RESOREX[10]. The factor g on C is determined by the number of missing near neighbours to the fuel rod in question, i.e.

$$g = \begin{cases} 1 & \text{for interior rods,} \\ \frac{5}{8} & \text{for edge rods,} \\ \frac{3}{8} & \text{for corner rods.} \end{cases}$$

The resulting Dancoff corrections for the three cases of different void contents are shown in table 5.1.a. The numbers of the fuel rods refer to the composition numbers of fig. 5.1.a. The value of the resonance absorption cross section of U^{238} is in CDB multiplied by the factor DC, which means that the production of Pu^{239} is increased for the edge and corner rods. In this respect no difference is made between fuel rods adjacent to the broad and narrow water gaps, because even the narrow water gaps are considered to be broad enough to make the shielding from the fuel in the next assembly negligible.

Table 5.1.a.

Dancoff corrections for CDB calculations

Void content	1 - C	C	DC, g = 1 Rod no. 9	DC, g = 5/8 Rod nos. 7, 8	DC, g = 3/8 Rod nos. 4-6
0%	0.7352	0.2648	1	1.066	1.107
25%	0.6562	0.3438	1	1.094	1.152
50%	0.5437	0.4563	1	1.146	1.234

5.2. Comparisons with Other Calculations

In ref. 16 a series of calculations for the DRESDEN 1 reactor run by Combustion Engineering is reported. The purpose of these burn-up calculations was to produce input data for the overall nodal code FLARE[17]. FLARE requires as input the beginning-of-life k_∞ and the migration area M^2, and these quantities are therefore given in the report for the three void levels of the calculations. In table 5.2.a. our calculated k_{eff}, k_∞ and M^2 from the CDB box calculations are shown and compared with the Combustion Engineering calculated values of k_∞ and M^2. The corresponding values from the CEB unit cell are likewise given. k_∞ is the value calculated with zero buckling, whereas the k_{eff} is obtained by putting the overall buckling $B_g^2 = 0.00033\ cm^{-2}$. M^2 has been calculated on the basis of the homogenized 2-group cross sections from CEB and CDB respectively.

The combustion Engineering calculations of isotopic depletion are given in ref. 16 for exposures up to 30000 MWD/TU. In figs. 5.2.a. and 5.2.b. the box-average number densities as a function of burn-up calculated by CDB for the 0 void case are shown together with the corresponding curves from ref. 16. The degree of agreement was quite similar in the cases of 25% and 50% void.

Measured values of isotopic compositions are only available in very few points for exposure values greater than 10000 MWD/TU; up to that value the agreement in the two calculation sets is pretty good. In ref. 15, however, some measurements are reported for first core fuel elements which have been irradiated in the core during the succeeding fuel cycles up to an exposure of 20000 MWD/TU before the analysis. Nothing in the measurements indicates that the concentration of Pu^{239} falls off drastically after 10000 MWD/TU. For comparisons with the measurements see section 5.3.

A possible explanation of the discrepancy in the Pu build-up might be that the Combustion Engineering calculations were performed for a pin cell equivalent to the average box, i.e. a unit cell in which the influence from the water gaps round the box was accounted for in some approximate way. If, for instance, water from the inter-box gaps is placed around the asymptotic unit cell, its influence on the depletion is overestimated with the result that the Pu-production is lowered. To check this an "equivalent unit cell" was constructed by simply increasing the cell radius so that the amount of extra water corresponded to sharing the water from the gaps equally between the pins. The results of the depletion of the equivalent cell is also

Table 5.2.a.

k_{eff}, k_{∞} and M^2 for the unrodded fuel box at hot, clean full power conditions

	k_{eff}	k_{∞}	M^2 cm^2	
Combustion Engineering	-	1.1414	56.402	0% void
CDB, box	1.1157	1.1376	59.420	
CEB, asymptotic pin	1.0985	1.1202	59.450	

	k_{eff}	k_{∞}	M^2 cm^2	
Combustion Engineering	-	1.1263	70.676	25% void
CDB, box	1.0968	1.1232	72.824	
CEB, asymptotic pin	1.0426	1.0706	81.137	

	k_{eff}	k_{∞}	M^2 cm^2	
Combustion Engineering	-	1.0999	92.590	50% void
CDB, box	1.0647	1.0971	92.130	
CEB, asymptotic pin	0.9438	0.9814	120.13	

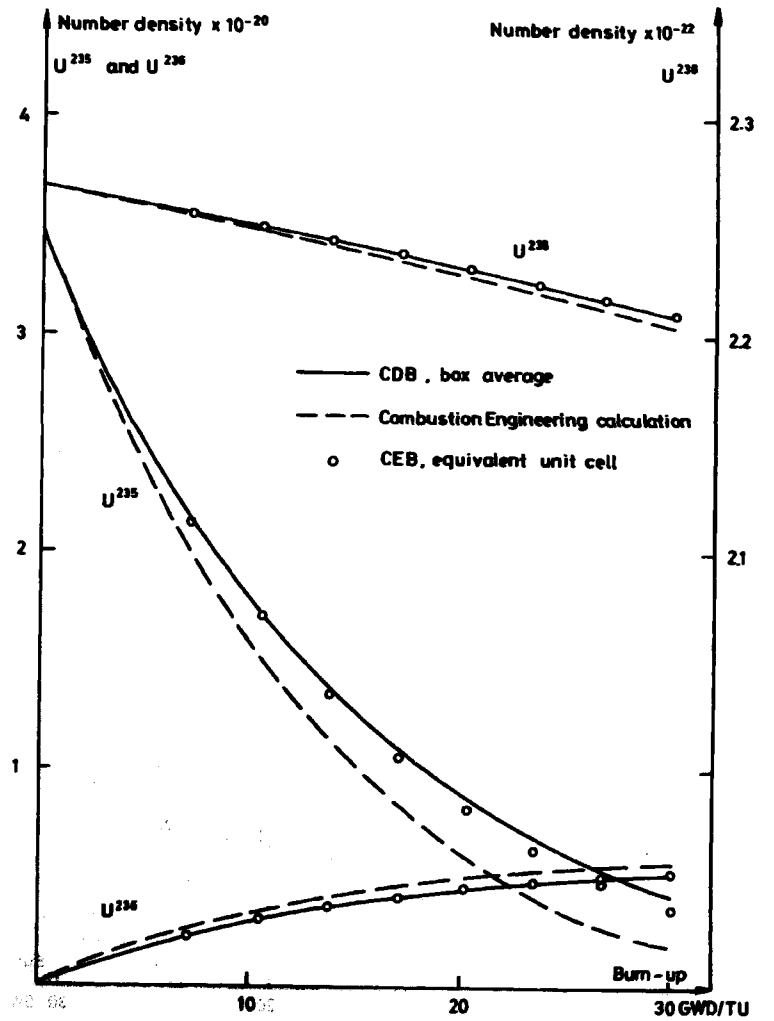

Fig. 5.2.a. DRESDEN 1. Calculated box-average isotopic depletion 0 % void.

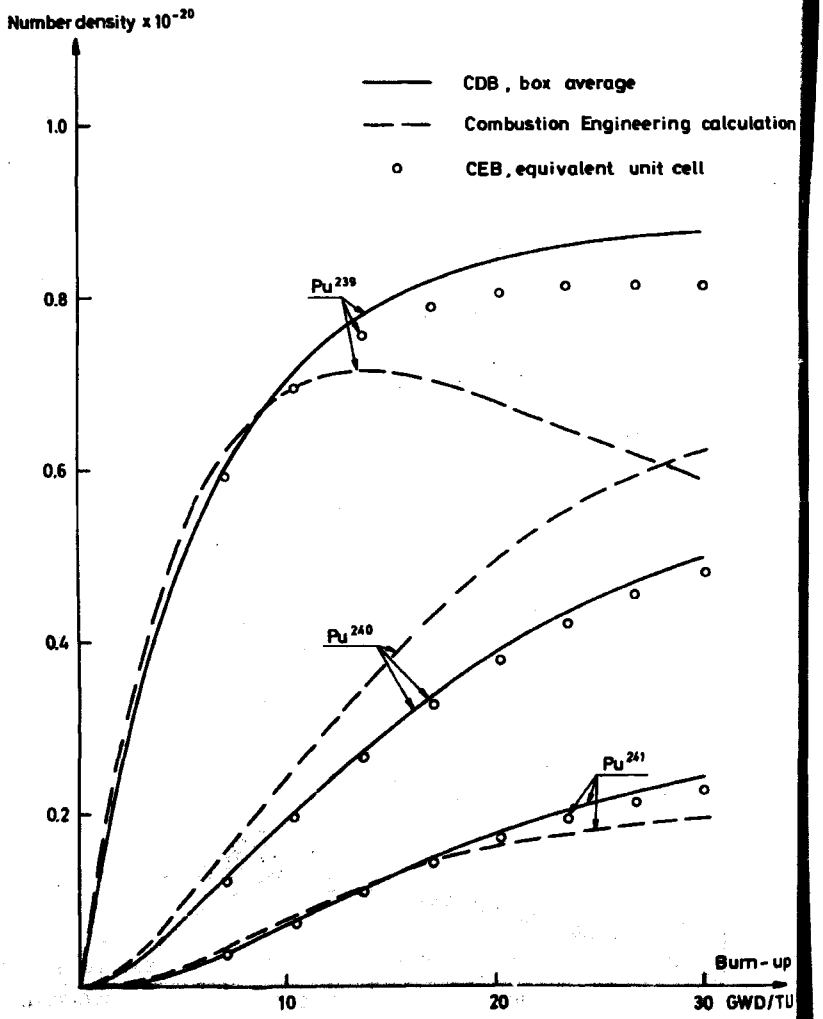

Fig. 5.3.a. BRESDEN 1. Calculated box-average isotopic depletion. 0% void.

shown in the figures. Even though a tendency in the direction of the Combustion Engineering calculation is present, the depletion of the equivalent unit cell still looks more like the CDB box results. The reason for the large discrepancy is therefore most likely to be found in the cross section data.

The k_{eff} of our equivalent unit cell was about 3% too high for all burn-up values compared to the 0 void box calculation with the same detailed FIPO fission product treatment. In this connection the very good agreement between the beginning-of-life infinite multiplication factors, k_∞, of the CDB and Combustion Engineering calculations should be noted.

5.3. Comparisons with Measurements

The appearance of k_{eff} calculated by CDB as a function of burn-up is shown in fig. 5.3.a. for the three different void contents considered. It may be noted that the curves intersect at high burn-up values because of the lower production of Pu in the more well-moderated low-void cases, but it must be remembered that for exposures higher than 15000 MWD/TU the calculated values of k_{eff} may be far from the truth owing to the fission product treatment as shown in section 4.1. So the results between 20000 and 30000 are only suitable for mutual comparisons.

The intersection between the k_{eff}-curves and the line $k_{eff} = 1$ may be compared with the observed average exposure of core 1 at the end of the first fuel cycle, which is obtained from ref. 18. At reactor shut-down, the average exposure was 4927 MWDt/short ton U. The exposure worth of the power shaping control rods partially inserted in the core at the end of cycle 1 and one rod fully inserted due to malfunction is in ref. 18 estimated to be 445 MWDt/short ton U. By adding these two values and multiplying by $\frac{1000}{907.2}$ the theoretical end-of-life average exposure in MWD thermal per metric ton of U is found to be 5922 MWD/TU.

A more correct value for comparisons with the box calculations should be slightly smaller, because the reactor was run at half power during a short period after reactor start-up and at derated power for the last 550 MWD/TU. As seen from fig. 5.3.a. the end-of-life average exposure of core 1 falls as expected a little before the intersection point of the mean void calculated k_{eff} and the line of unity.

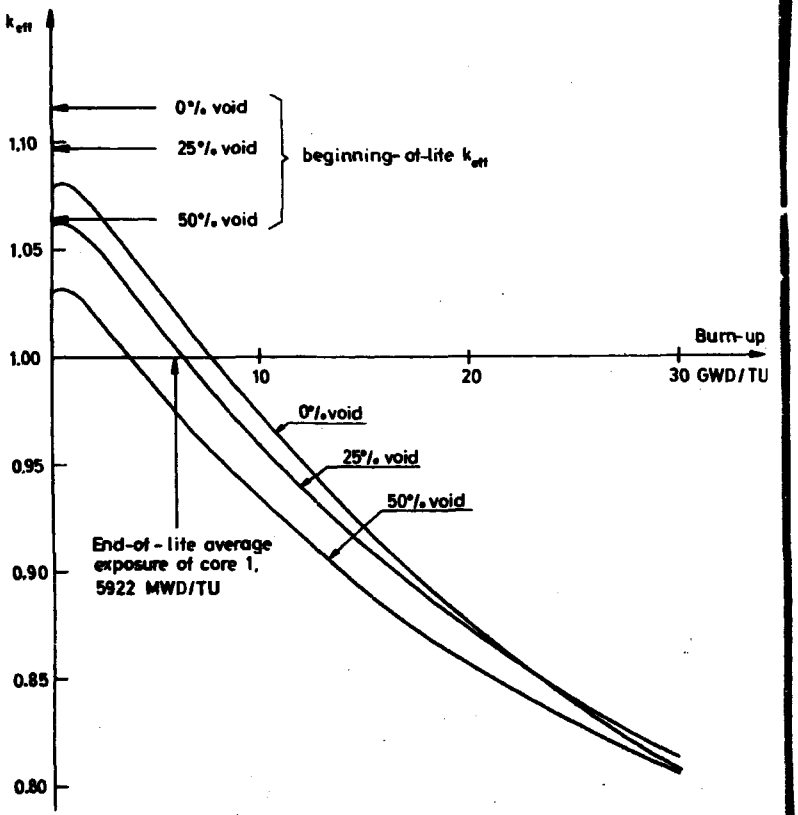

Fig. 5.3.a. k_{eff} versus burn-up for DRESDEN 1 fuel box. CDB calculations, hot, full power.

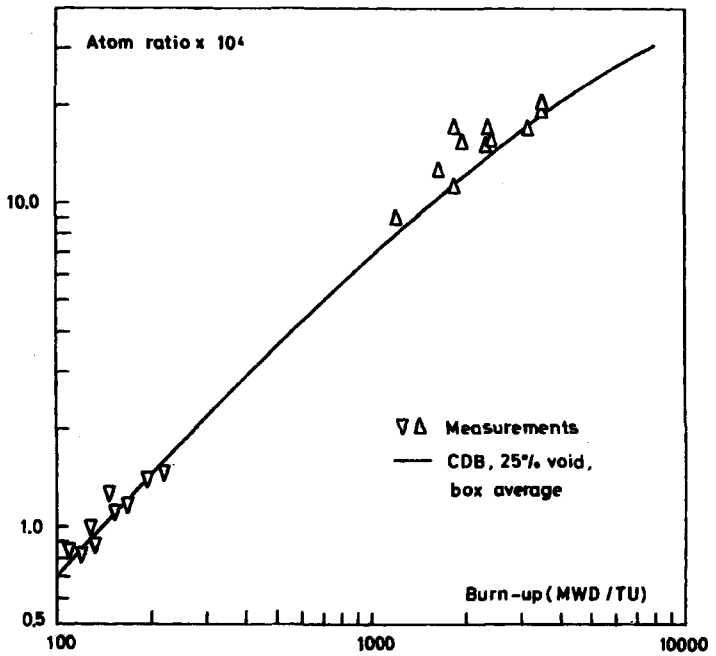

Fig. 5.3.b. Pu^{239}/U^{238} atom ratio versus burn-up.

Table 5.3.a.

Fuel assembly power peaking factors

		Power form factor
CDB box calculation	0% void	1.318
Beginning-of-life	25% void	1.337
	50% void	1.347
Gamma scan measurement, ref. 19		less than 1.39

During the early operation of the DRESDEN 1 reactor the power distribution for the core and for the fuel assemblies was tested by gamma activity measurements to ensure that the power peaking factors allowed full power operation. In ref. 19 is reported the results of gamma scan measurements of a fuel assembly irradiated in the core during the first 4000 MWD of operation. Table 5.3.a. gives the CDB calculated power peaking factors at beginning of life. The calculations are in agreement with the conclusion of ref. 19 to the effect that the power peaking factor in the DRESDEN 1 first core fuel element must be less than 1.39.

To determine experimentally the initial conversion ratio of the DRESDEN 1 fuel a test element was inserted during the initial reactor operation and discharged for analysis after an exposure of 100-200 MWD/TU. After the end of cycle 1, a number of fuel samples irradiated to 1000-3500 MWD/TU were collected and analyzed. The results of isotopic composition measurements from these two experimental series are reported in ref. 14.

The samples were taken from different positions in the fuel assembly and from fuel elements with different histories as to control rod movements. As no information is given as to which irradiation history belongs to the individual measuring points the best thing to do is to compare the measurements with the CDB box average calculations for mean void, i.e. 25%. The experimental uncertainties are estimated in ref. 14 to be

1-1 $\frac{1}{2}$% for ratios of the isotopes of U

1-1 $\frac{1}{2}$% for ratios for the isotopes of Pu,

2-5% for the Pu/U ratio,

6% for the concentration of burn-up indicators.

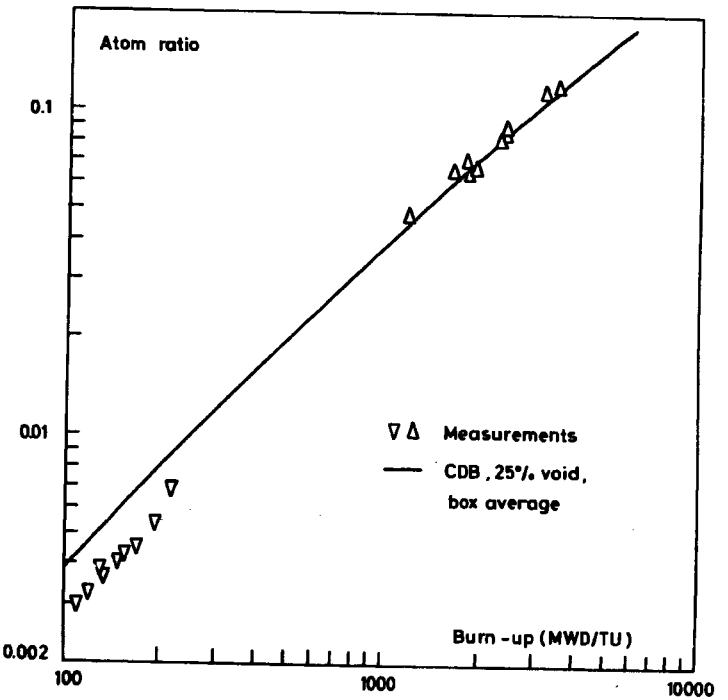

Fig.5.3.c. Pu^{240}/Pu^{239} atom ratio versus burn-up.

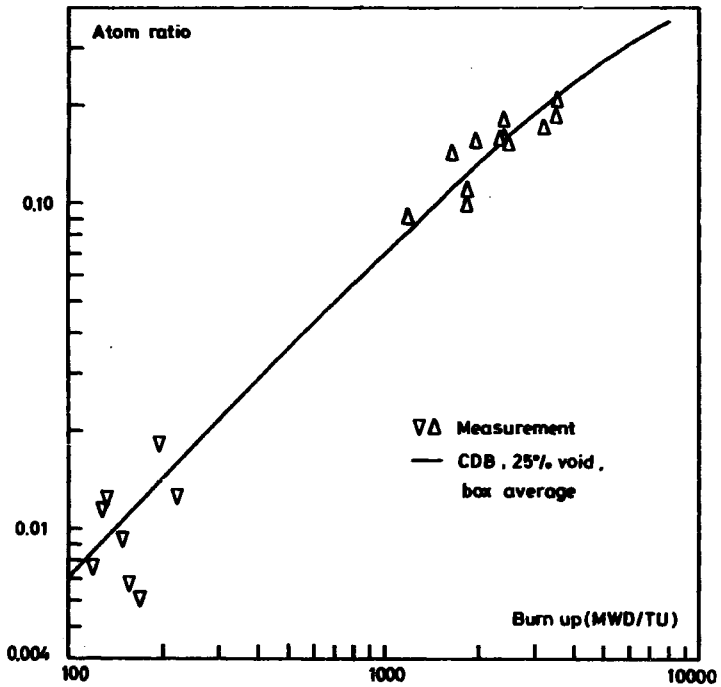

Fig. 5.3 d. Pu^{241} / Pu^{240} atom ratio versus burn-up.

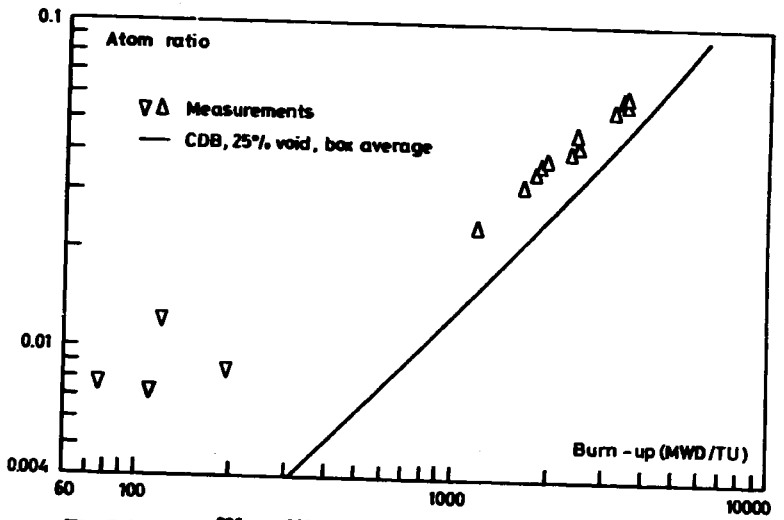

Fig. 5.3.e. U^{236} / U^{235} atom ratio versus burn-up.

The measured values are given as the concentration ratios of pairs of succeeding isotopes in the depletion chains versus exposure. The comparisons with the CDB calculated values are shown in figs. 5.3.b.-5.3.e.

Fig. 5.3.b. shows the Pu^{239}/U^{238} atom ratio as a function of burn-up. The agreement is good, but there is a tendency to slightly underestimate the ratio for higher exposures, which might be interesting compared with fig. 5.3.c., showing a clear overprediction in the calculations of the Pu^{240}/Pu^{239} ratio at very low exposures. At the low Pu^{240} concentrations at the beginning of irradiation, the atom ratio of Pu^{240} to Pu^{239} is determined mainly by the capture rate of Pu^{239}, and a too high Pu^{239} capture cross section might as well explain a low Pu^{239}/U^{238} atom ratio at higher exposures. However, the discrepancies are not large enough to allow definitive conclusions concerning cross sections.

About the Pu^{241}/Pu^{240} ratio of fig. 5.3.d. the only thing to say is that the agreement between calculation and measurements is quite satisfying. This is not the case in fig. 5.3.e. where the calculated ratio of U^{236} to U^{235} is lying far below the measured values. The reason for this discrepancy is that the initial content of U^{236} in the fuel was ignored in the calculations. At the low exposures the experimental points are simply a measure of the initial U^{236} concentration, which was set to zero in the calculations. According to ref. 14 the initial enrichment of U^{236} is still the cause of 10% of the total U^{236}/U^{235} atom ratio at the exposure of the last experimental point. This explains about half of the deviation at 3500 MWD/TU.

The measurements of the Pu^{242}/Pu^{241} atom ratio from ref. 14 were omitted here because of the lack of data for Pu^{242} in the calculations.

In ref. 15 isotopic composition measurements are given for fuel from the first core irradiated in the subsequent cores to exposures of up to 20000 MWD/TU. The samples were taken at four axial positions from the fuel element and come partly from corner rods and partly from rods in the middle of the assembly. Most of the samples are taken from the corner rods because they are easier to remove.

The fuel elements from which the samples were taken were most of the time operated in the core with the adjacent control rods withdrawn. However, the dispersion in measuring results may partly be explained by the unknown influence from control rods. The corner rod samples were taken from the corner with the greatest water gap, i.e. at the control rod position, but according to ref. 15 some of the fuel elements were rotated at refuelling so that they were partly irradiated at the narrow water gaps.

Only the data from three of the four axial positions were used for the present comparison. These were data from the top of the core, corresponding to maximal void, the data from position II, corresponding to average void, and the data from the bottom, corresponding to no void. The measured ratios of total Pu to U^{238} concentrations were compared with the CDB calculated values for 0%, 25% and 50% void respectively. The corner rod of the calculations was the fuel rod type 4, and for the interior rods the calculated isotopic compositions of rod type 9 were used (see fig. 5.1.a.).

In the case of interior rods only average void measurements were given. These are shown together with the CDB 25% void results in fig. 5.3.f. In fig. 5.3.g. the corner rod data are compared with the 0%, 25% and 50% void calculated curves for the corner pin. The measured points are somewhat dispersed due to the varying irradiation conditions mentioned above, but nevertheless the agreement between calculation and measurements is quite satisfying.

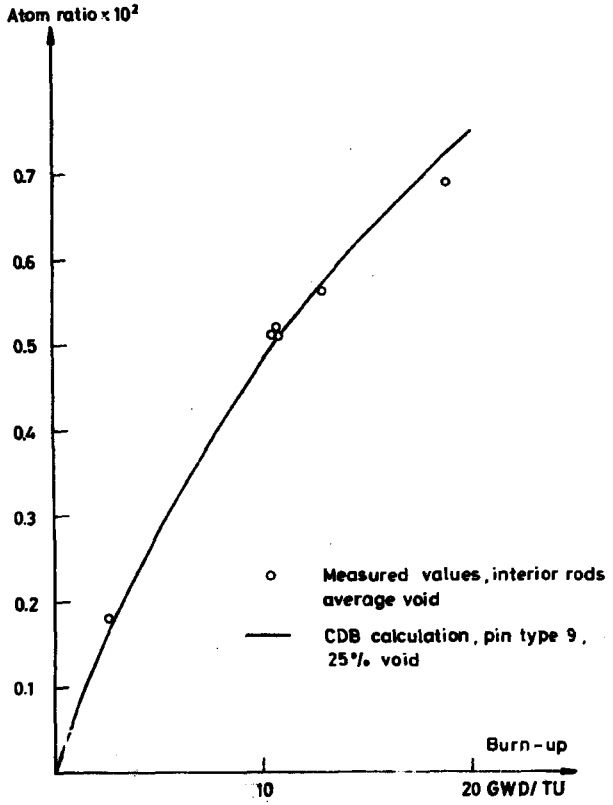

Fig. 5.3.f. Total Pu/U^{238} atom ratio versus burn-up. Interior rods.

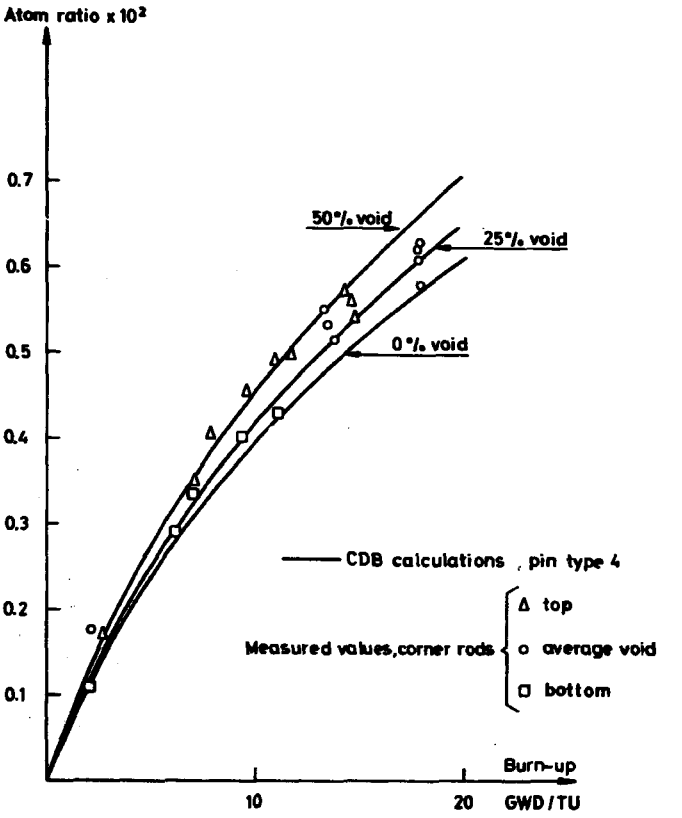

Fig. 5.3.g. Total Pu/U^{238} atom ratio versus burn-up. Corner rods.

6. CONTROL RODS

In the box burn-up program CDB, the power distribution is found by using the diffusion theory procedure TWODIM. When a control rod is present, the use of diffusion theory, without special treatment of the control rod, is not justified. Some authors claim that even when a control rod is not present will the rather broad water gaps surrounding the fuel box necessitate a better treatment, since diffusion theory will not represent the effect of these gaps correctly.

In order to estimate the errors introduced in using diffusion theory, a number of computations have been carried out on a typical DRESDEN 1 fuel box, comparing diffusion theory and S_4 theory. The choice of a S_4 calculation to carry out reference calculations has not been made because the S_4 theory yields the correct answers, since it is still an approximate method. But the S_4 calculation with isotropic scattering is a realistic alternative to diffusion theory in a burn-up code and it is believed to give better results.

6.1. Cross Sections for Control Rods

The cross sections for the B-SS control rods are obtained by means of CRS program[6]. The reduction of the 76-group cross sections from CRS to 5-group cross sections is carried out in a similar way as is the reduction for the water gaps. A one-dimensional collision probability calculation has been performed with the GP program[13] in a geometry shown in fig. 6.1.a. The spectrum thus obtained is used to calculate 5-group cross sections, both for the control rod and the nearby water gap. In the same calculation a set of homogenized cross sections for the control rod and the same water gap has been found.

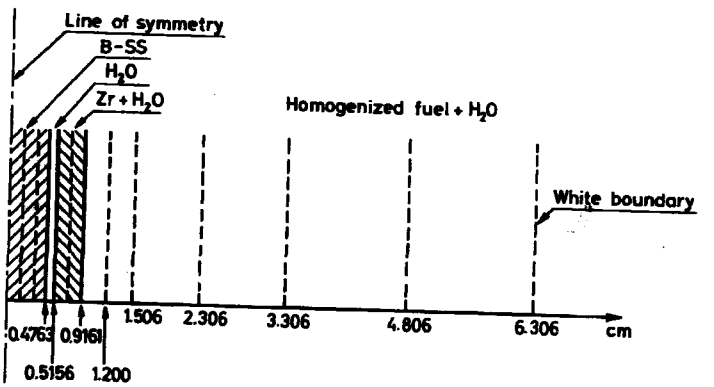

Fig. 6.1.a. Material compositions and mesh division for slab geometry calculation of few-group cross sections for control rod.

6.2. S_4 Calculations

For the S_4 calculations has been used the S_N code TWOTRAN[20] with isotropic scattering and reflecting boundary conditions at the outer surfaces of the box. The scattering cross sections have to be transport corrected in the usual way. The geometry is shown in fig. 6.2.a. The actual size of the box can be found elsewhere in this report. Two calculations have been carried out. One, as shown, with a control rod, and one in which the control rod is replaced by H_2O.

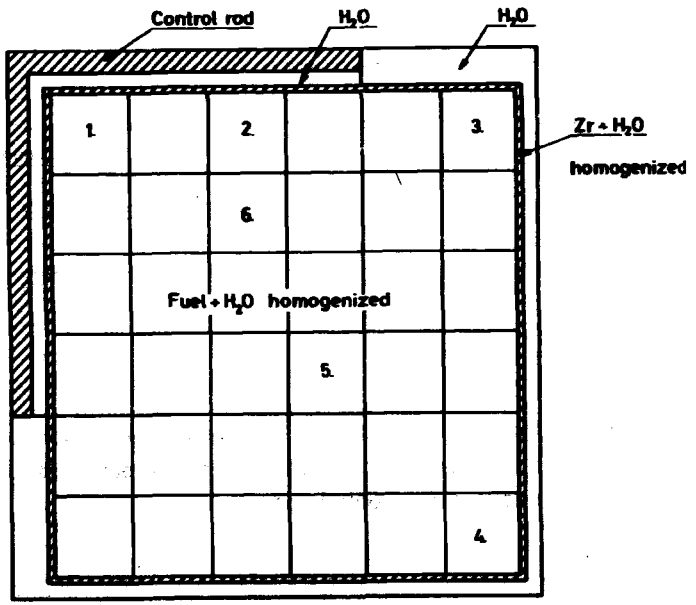

Fig. 6.2.a. Dresden I fuel box. Geometry for S_4 and diffusion calculation.

6.3. Diffusion Calculations

In this case the progam Diff 2D based on the TWODIM procedure[21] has been used. In the same geometry as before (fig. 6.2.a.) with the control rod present, two calculations have been carried out. In the first, the homogenized cross section set for the control rod and the water gap between the control rod and the $Zr + H_2O$ zone has been used. In the second, the control rod and water gap were considered an outer zone to the fuel box. In this case a set of boundary conditions for the interface between the $Zr + H_2O$ and water gap was used.

The boundary is represented by a Y-matrix; a Y-matrix is defined by the equation

$$\underline{J} = \underline{Y}\ \underline{\Phi},$$

where $\underline{J}$ and $\underline{\Phi}$ are column vectors containing the group currents and group fluxes on the boundary. The Y-matrix is calculated by the collision probability code HECS[22].

For the unrodded box two similar computations have been performed. Only, in this case, the representation by Y-matrices has been extended to all water gaps around the box.

6.4. Results

In all cases, the flux was normalized in such a way that the power levels were the same. The results are found in table 6.4.a., 6.4.b. and 6.4.c. The mesh numbers refer to the numbers in fig. 6.2.a.

Finally it should be mentioned that the increase of the order of N in the S_N calculation does not seem to alter the results for the DRESDEN 1 fuel box significantly.

Table 6.4.a.

Comparisons between power distribution calculated by S_4 theory and diffusion theory. DRESDEN 1. Unrodded box

Mesh no.	Power deviation $(P_{diff} - P_{S_4})/P_{S_4}$ (%) Water gaps repr. by cross sect.	Power deviation $(P_{diff} - P_{S_4})/P_{S_4}$ (%) Water gaps repr. by Y-matrices
1	+ 1.07	+ 0.80
2	- 1.86	- 2.25
3	- 0.81	- 0.59
4	- 2.54	- 2.22
5	- 4.70	- 4.60
6	- 3.35	- 3.43

Table 6.4.b.

Comparisons between power distribution calculated by S_4 theory and diffusion theory. DRESDEN 1. Box with control rod.

Mesh no.	Power deviation $(P_{diff} - P_{S_4})/P_{S_4}$ (%) Control rods repr. by cross sect.	Power deviation $(P_{diff} - P_{S_4})/P_{S_4}$ (%) Control rods repr. by Y-matrix
1	- 20.5	- 0.82
2	- 12.6	- 2.94
3	+ 7.54	+ 4.88
4	+ 4.69	+ 1.20
5	+ 0.31	- 1.41
6	+ 6.17	- 2.83

Table 6.4.c.

Comparisons between the effective multiplication constant k_{eff} for the DRESDEN 1 fuel box calculated by S_4 theory and diffusion theory

	S_4 theory	Diffusion theory cross sect.	Diffusion theory Y-matrix
Box with control rod	0.8225	0.8131	0.8271
Unrodded box	1.1168	1.1155	1.1294

6.5. Conclusion

Two conclusions can immediately be drawn. For the unrodded box, the somewhat more elaborate method of first finding a Y-matrix and then doing a diffusion calculation is not justified. The improvements in the determination of the power distribution are rather small, and the reactivity seems to be even more in error than without the Y-matrices.

For the fuel box with a control rod, the use of a Y-matrix does improve the results considerably, and it seems reasonable to treat a rodded box by diffusion theory only, if the control rod itself is treated by a better method than by diffusion theory.

If one treats the unrodded box by diffusion theory, and the rodded box by diffusion theory and Y-matrices, the deviations from an S_4 calculation are within 5% in the power distribution. Since S_4 calculation need not yield the correct results, and since experimental data for direct comparison have not been available, the use of diffusion calculations in this case seems to be reasonable.

7. SYNTRON/VOID A THREE-DIMENSIONAL OVERALL BURN-UP PROGRAM

For the overall calculation at the DRESDEN 1 reactor the SYNTRON/VOID program has been used. In this section a brief description of this program will be given.

The SYNTRON/VOID program consists of the following three main blocks: multi-group flux and power distribution calculations, multi-channel void and temperature calculations, and burn-up calculations based on the interpolation principle.

For the multi-group flux calculations the three-dimensional flux synthesis program SYNTRON[23] is used. The SYNTRON program is a single channel variational flux synthesis program primarily based on Kaplan's method[24]. Besides the actual synthesis, the program contains a routine for the calculation of the two-dimensional expansion functions by use of the ordinary difference equation technique. The three-dimensional flux distribution $\varphi^g(z, y, x)$ is found by the expansion of $\varphi^g(z, y, x)$ after some two-dimensional flux functions, $H_k^g(y, x)$, called trial functions; (z) is the axial and (y, x) the radial directions. The trial functions are calculated by using the two-dimensional difference equation routine.

As described in ref. 23 the group flux $\varphi^g(z, y, x)$ is found by means of the following expansion:

$$\varphi^g(z, y, x) = \sum_{k=1}^{K_g} Z_k^g(z) \cdot H_k^g(y, x) , \qquad (7.1)$$

where

K_g = number of trial functions in group g

$H_k^g(y, x)$ = trial function number k in group g

$Z_k^g(z)$ = mixing function number k in group g.

The methods used for the multi-channel void and temperature calculations are described in the following section in this report. For the void calculations the reactor is divided into some parallel channels; typically each channel consists of four fuel boxes with a control rod in the middle. On the basis of an input power distribution the void routines calculate the void and temperature distributions up through each channel.

A quasi-stationary burn-up treatment is used in the program. The power, void and temperature distributions are held constant during each burn-up step.

The cross sections for the burnable materials in the reactor are taken from a precalculated burn-up table. The cross sections in the burn-up table represent macroscopic homogenized box cross sections. Different burn-up tables are allowed for different types of fuel boxes, viz. boxes with and without control rod and boxes with different enrichment. The burn-up tables are limited to three dimensions, i.e. to three interpolation parameters. To find the actual cross sections for a flux calculation linear interpolation in the three-dimensional parameter space is performed for each

burn-up region in the reactor. Commonly the following interpolation parameters are used: burn-up in MWD/TU, average void during the burn-up and the actual void content.

In addition to the cross section interpolation the SYNTRON/VOID program contains some routines for adjustment of the tabulated cross sections.

The cross section tables are assumed to be calculated with constant power and fuel temperature during the burn-up, reference values.

The deviation between the reference fuel temperature and the actual fuel temperature, the Doppler effect, is taken into account by a polynomial correction to the interpolated cross sections. In a two-energy-group treatment the Doppler corrections are put on the fast absorption cross section and the removal cross section. These cross sections are selected because the influence of the Doppler effect is most significant for the resonances in U^{238}, and in our two-group treatment with the boundary between fast and thermal groups at 1.855 eV these resonances are found in the fast group.

The correction polynomials have the following form:

$$\Delta\Sigma = (A1 + A2 \cdot BU) \cdot (1 + A3 \cdot a + A4 \cdot a^2) \cdot (\sqrt{T} - \sqrt{T_{ref}}). \qquad (7.2)$$

Where A1...A4 are input coefficients, BU burn-up in MWD/TU, a the actual void fraction, and T_{ref} and T are respectively reference fuel temperature and actual fuel temperature in degree absolute. Later in this report further argumentation for the use of this polynomial is given.

The cross section tables are assumed to be generated with an equilibrium xenon term included. If the actual power level is different from the reference power the xenon content change. To account for this effect an equilibrium xenon term is implemented. The equilibrium xenon concentration is given by the following expression[25]

$$n_{Xe,\,eq} = \frac{(\gamma_I + \gamma_{Xe}) \cdot \Sigma_f \cdot \varphi}{\lambda_{Xe} + \sigma_{a,Xe} \cdot \varphi} , \qquad (7.3)$$

where λ is the decay constant, γ the fission yield, σ_a the microscopic absorption cross section and φ the group flux. Σ_f is the macroscopic fission cross section. $\sigma_a\varphi$ is supposed to include summation over all energy groups. Similarly, $\gamma\Sigma_f\varphi$ includes summation over all energy groups.

The correction term is then

$$\Delta\Sigma_a = \sigma_{a,Xe} \cdot (n_{Xe,\,eq\,actual} - n_{Xe,\,eq\,ref}) \cdot \qquad (7.4)$$

Besides this equilibrium xenon treatment, the program contains a routine for non-equilibrium xenon treatment[26]. This routine is used for investigations of xenon-induced spatial power oscillations.

The calculation scheme for the SYNTRON/VOID program is shown in fig. 7.a. The calculation starts with a guessed power distribution, or the previous power distribution if the job is restarted. As the void distribution exerts a drastic influence on the power distribution the coupling between void and power is underrelaxated.

The SYNTRON/VOID program is more detailed described in refs. 27 and 28.

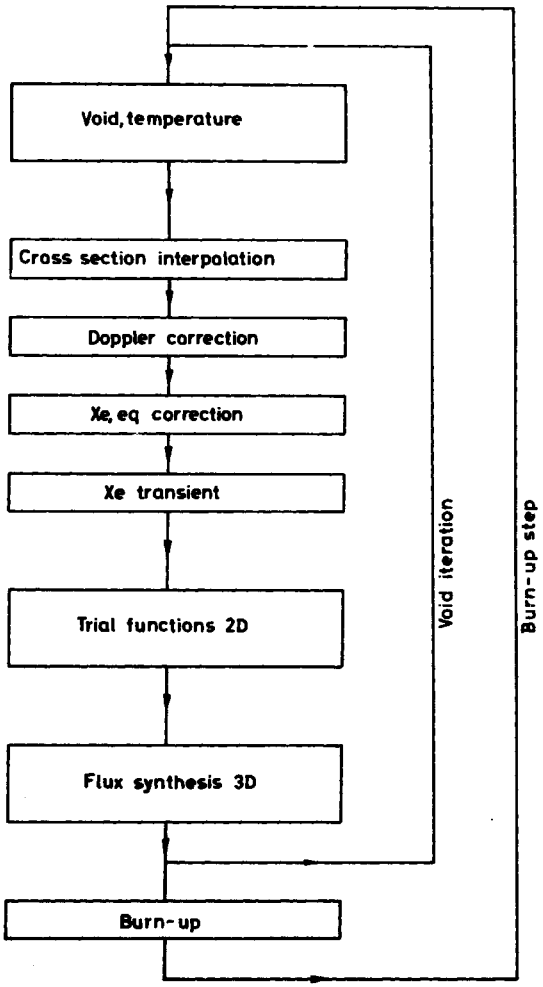

Fig. 7.a. The SYNTRON/VOID program.

8. HYDRAULICS

The typical design of a BWR core makes the calculation of the hydraulic performance somewhat simpler than that of a PWR core, since the flow in the channels can be treated one-dimensional.

8.1. Flow in a Single Vertical Channel

The equations for the flow in a single channel are derived from the three-dimensional equations. To describe the flow, we have three conservation equations of the type

$$\frac{\partial \rho}{\partial t} + \nabla \cdot \underline{J} = S \qquad (8.1)$$

for the property ρ, where S is a source, and

$$\underline{J} = \rho \underline{v}$$

and $\underline{v}$ a velocity vector.

Since the flow is considered one-dimensional and since we only deal with steady state conditions, (8.1) can be reduced to

$$\frac{\partial}{\partial z}(\rho v_z) = S. \qquad (8.2)$$

(8.2) is now used for mass, energy and momentum.

Since we have two-phase flow, the equations become

for mass:

$$\frac{\partial}{\partial z}[(1-\alpha)\rho_f v_f + \alpha \rho_g v_g] = 0 \qquad (8.3)$$

for energy:

$$\frac{\partial}{\partial z}[(1-\alpha)\rho_f v_f h_f + \alpha \rho_g v_g h_g] = q/A \qquad (8.4)$$

for momentum:

$$\frac{\partial}{\partial z}[(1-\alpha)\rho_f v_f^2 + \alpha \rho_g v_g^2] = \frac{\partial p}{\partial z} - g[(1-\alpha)\rho_f + \alpha \rho_g] - \frac{\partial F}{\partial z} \qquad (8.5)$$

where

- α is void fraction
- v is velocity
- ρ is density
- h is specific enthalpy
- A is cross section area of channel
- q is heat input per unit length
- g is gravity
- $\frac{\partial F}{\partial z}$ is friction force per unit length and unit area

and subscripts f and g refer to water and steam respectively.

For $\frac{\partial F}{\partial z}$ is used

$$\frac{\partial F}{\partial z} = f R \rho_f v_f^2 .$$

The friction factor f is

$$f = \frac{C_1}{2 D R_e^{C_2}},$$

where

- C_1 and c_2 are constants,
- D is the hydraulic diameter
- R_e is the Reynolds number;

f becomes the Weisbach's formula for smooth pipes for $C_1 = 0.184$ and $c_2 = 0.2$.

The two-phase friction factor R is, according to Becker,

$$R = 1 + 2400 \left(\frac{x}{p}\right)^{0.95},$$

where

x is the steam quality

p is the pressure in ata.

Since boiling takes place along the channel, we also have the equation

$$\frac{\partial}{\partial z}\left[\alpha v_g + (1-\alpha) v_f\right] = \left(\frac{1}{\rho_g} - \frac{1}{\rho_f}\right)\Phi, \tag{8.6}$$

where Φ is the evaporation rate per unit volume; (8.6) expresses conservation of volume.

When solving (8.3) and (8.6) we have the three unknown v_f, v_g and α, that is we must have a third equation. This is

$$v_g = S v_f + v_o, \tag{8.7}$$

where the Solberg slip formula[30]

$$S = S_1 + S_2 \alpha^r$$

is used.

The steam velocity due to the buoyancy v_o is determined from

$$v_o = -S_g \cos\varphi,$$

where φ is the angle between the gravity and the direction of flow. S_1, S_2, S_g and r are input constants.

Lastly we must have a model for boiling, which will be discussed in the next part of this chapter.

8.2. Models for Boiling and Heat Transfer

The boiling model used is the Ramona boiling model[30]; this is

$$\Gamma = \Gamma_B + \Gamma_{SF}.$$

Γ is the total evaporation rate, Γ_B is the bulk boiling and Γ_{SF} is the boiling at the heat transfer surface.

For the bulk term is used

$$\Gamma_B = \frac{V f (T - T_s)}{h_{fg}}, \tag{8.8}$$

where

V is the volume in which boiling takes place

T is the temperature of the water

T_s is the saturation temperature

h_{fg} is the evaporation enthalpy

and

$$f = \begin{cases} [R_o + R_1 \alpha(1-\alpha)](1+\varkappa) & \text{for } T > T_s \\ [R_o + R_1 \alpha(1-\alpha)](1-\varkappa) & \text{for } T < T_s, \end{cases} \tag{8.9}$$

where R_o, R_1 and $\varkappa$ are constants.

The model describes both boiling and condensing, and it is seen that these processes take place at different rates if $\varkappa \neq 0$.

The surface term is obtained from

$$\Gamma_{SF} = \frac{Q^*}{h_{fg} + C_p(T_s - T)\frac{\rho_f}{\rho_g} + \frac{1}{2} C_p (T_{ca} - T_s)\frac{\rho_f}{\rho_m}}, \tag{8.10}$$

where

C_p is the specific heat at constant pressure

T_{ca} is the heat transfer surface temperature

$$\frac{1}{\rho_m} = \frac{1}{\rho_g} - \frac{1}{\rho_f}.$$

Q^* is determined from

$$Q^* = \begin{cases} A_s K_B (T_{ca} - T_s)^4 & \text{for } T_{ca} > T_s \\ 0 & \text{for } T_{ca} < T_s, \end{cases} \tag{8.11}$$

where

$$K_B = 1.266\, e^{1.61 \cdot 10^{-7} p}$$

p is the pressure in N/m^2

A_s is the heat transfer surface area.

(8.11) is the Jens-Lottes correlation for boiling heat transfer.

T_{ca} is calculated from

$$T_{ca} = \min. \begin{cases} T_s + \frac{1}{K_B}\left(\frac{Q(1-\delta)}{A_s}\right)^{0.25} \\ T + \frac{1}{K_{NB}} \frac{Q(1-\delta)}{A_s} \end{cases} \qquad (8.12)$$

where

Q is the power

δ is the fractions of energy released as γ-energy.

K_{NB} is the Colburn singlephase heat transfer coefficient:

$$K_{NB} = 0.023 \frac{|\rho_f v_{f,ci}|^{0.8} C_p^{0.4} \lambda_f^{0.6}}{\eta_f^{0.4} D_h^{0.2}},$$

where

$v_{f,ci}$ is the velocity at the channel inlet

λ_f is the thermal conductivity of the water

η_f is the dynamic viscosity

D_h is the hydraulic diameter.

8.3. Numerical solution

Only a few remarks on the numerical solution developed in ref. 31 shall be made.

The equations (8.3) to (8.6) will be reformulated and discretized.

The channels are divided into a number of nodes, and all the quantities are evaluated at the boundary between the nodes. Properties calculated like this are ascribed to all the preceding node.

At first we introduce the mass flow rates

$$w_f = A(1-\alpha)\rho_f v_f$$

$$w_g = A\alpha\rho_g v_f,$$

and the energy flow rates

$$w_{ef} = h_f w_f,\ w_{eg} = h_g w_g,\ w_e = w_{ef} + w_{eg}.$$

The enthalpies are

$$h_f = e_f + p/\rho_f = C_p(T-T_o) + p/\rho_f$$

$$h_g = e_g + p/\rho_g = C_p(T_s-T_o) + h_{fg} + p/\rho_f,$$

where T_o is some arbitrarily selected reference temperature and where we have used the relationship

$$C_p(T_s-T_o) + h_{fg} = e_g + p/\rho_m.$$

Using k to indicate the node number, equations (8.3) and (8.6) can be written

$$w_{f,k} = w_{f,k-1} - \Gamma_k \qquad (8.13)$$

$$w_{g,k} = w_{g,k-1} + \Gamma_k, \qquad (8.14)$$

where Γ_k is the total evaporation rate in node k. Equation (8.4) is written

$$w_{e,k} = w_{e,k-1} + Q_k, \qquad (8.15)$$

where Q_k is the power dissipated in the k'th node.

By means of (8.13), (8.14), (8.15) and the different models discussed, one can find $w_{f,k}$, $w_{g,k}$ and $w_{e,k}$ when $w_{f,k-1}$, $w_{g,k-1}$, $w_{e,k-1}$ and Q_k are known.

Lastly, the pressure drop across the node is calculated, using equation (8.5).

The right-hand side of (8.5) yields the terms

$$-\Delta p_k - g[(1-\alpha_k)\rho_{f,k} + \alpha_k\rho_{g,k}] - \frac{\partial F}{\partial z}\Big|_k \Delta z_k.$$

Since α_k is the value at the boundary k, one will obtain a better result using

$$\bar{\alpha}_k = (\alpha_k + \alpha_{k-1})/2 .$$

The right-hand side then becomes

$$-\Delta p_k - g[\,(1-\bar{\alpha}_k)\rho_{f,k} + \bar{\alpha}_k \rho_{g,k}\,] - \left.\frac{\partial F}{\partial z}\right|_k \Delta z_k .$$

The left-hand side, the acceleration pressure drop, is written

$$U_k - U_{k-1} ,$$

where

$$U_k = \frac{1}{A}\,[w_{fk} v_{fk} + w_{gk} v_{gk}\,] .$$

If there are singularities in the channel (spacers, restrictions, expansions, etc.) these will be represented by

$$\Delta p_{sing} = \frac{1}{2} L U ,$$

where L is an input quantity which is positive for pressure drop in the flow direction, negative for pressure rise in the flow direction. Equation (8.5) then becomes

$$-\Delta p_k = g[\,(1-\bar{\alpha}_k)\,\rho_{f,k} + \bar{\alpha}_k \rho_{g,k}\,] + \left.\frac{\partial F}{\partial z}\right|_k \Delta z_k + (U_k - U_{k-1}) + \Delta p_{sing} \qquad (8.16)$$

8.4. Hydraulics Calculation for the Core

It has now been demonstrated how a flow calculation is performed for a single channel. In the core, we have several parallel coolant channels, and these are all surrounded by the moderator channel, i.e. there is heat exchange between the coolant channels and the moderator channel.

To take care of this, Q_k in equation (8.15) is modified to

$$Q_{k,j} = Q'_{k,j}\,(1-\delta) + k(T_{k,m} - T_{k,j}) + Q''_{k,j}$$

for the j'th coolant channel and

$$Q_{k,m} = k \sum_{j=1}^{N} (T_{k,j} - T_{k,m}) + Q''_{k,m}$$

for the moderator channel,

where

$Q'_{k,j}$ is the power in the j'th channel k'th node

k is the heat transfer coefficient for the shroud

N is the number of coolant channels

$Q''_{k,j}$ is the γ-energy absorbed in the water in the j'th channel k'th node given as

$$Q''_{k,j} = A_j(1-\alpha_{j,k})\,\delta \sum_{j=1}^{N} Q'_{k,j} \Big/ \sum_{j=1}^{N+1} A_j$$

A_j is the j, th channel cross section area and m = N+1.

First $T_{k,m}$ is set equal to $T_{k-1,m}$, and the $T_{k,j}$'s are computed. A new value of $T_{k,m}$ can now be found, and the process continues until it has converged.

An algol procedure VOIDN has been set up to solve the flow problem.

As input data, besides geometrical data and data for the various models used, must be given the inlet temperature, the pressure in the bottom of the core and the total mass flow rate

$$w_{tot} = \sum_{j=1}^{N} w_j + w_m .$$

The program then adjusts the mass flow rates w_j until the pressure drop across all the channels are equal within a prescribed accuracy.

In the program the properties of the water, T_s, ρ_f, ρ_g, h_{fg}, C_p, and λ are calculated from rational functions, taken from ref. 32. They are all calculated for saturation conditions at the given pressure.

8.5. The Fuel Model

The fuel model used is the same as that of the RAMONA code[30].

In the model, axial heat conduction is neglected, and the power is assumed to be generated uniformly throughout the fuel pellet cross section area.

The heat transfer from the fuel to the canning is given by

$$Q = -A\,K_1\,(T_{ca} - T_{fuelb})\,, \qquad (8.17)$$

where

A is the heat transfer area

T_{fuelb} is the temperature at the fuel surface.

The heat transfer coefficient K_1 is calculated from

$$K_1 = a_o + a_1\,\bar{T}_f + a_2\,\bar{T}_f^2 \qquad \text{and if}$$

$$a_o + a_1\,\bar{T}_f + a_2\,\bar{T}_f^2 \rangle\ a_3 \qquad \text{then } K_1 = a_3\,.$$

$\bar{T}_f$ is the fuel mean temperature.

The heat capacity of the gap and canning is assumed to be zero.

From the hydraulics calculation, T_{ca} is known, and from (8.17) T_{fuelb} can be determined.

The fuel temperature distribution is then found by solving the heat transmission equation

$$K_2\,\frac{\partial^2 T}{\partial r^2} + \frac{\partial K_2}{\partial r}\,\frac{\partial T}{\partial r} + K_2\,\frac{1}{r}\,\frac{\partial T}{\partial r} + Q = 0 \qquad (8.18)$$

subject to the boundary condition

$$T_{r=r_F} = T_{fuelb}$$

where

r_F is the outer radius of the fuel

K_2 is the conductivity of the fuel given as $K_2 = \dfrac{b_1}{1 + Tb_2}$

Q is the power density per unit area.

In order to solve (8.18), the equation is multiplied by $2\pi r$ and integrated from r_i to r_{i+1} ($r_{i+1} \rangle r_i$). One obtains

$$2\pi K_2\,r_{i+1}\,\frac{\partial T}{\partial r}\Big|_{r_{i+1}} - 2\pi K_2\,r_i\,\frac{\partial T}{\partial r}\Big|_{r_i} + \pi Q(r_{i+1}^2 - r_i^2) = 0\,. \qquad (8.19)$$

Taking T as linear between the centres of the zones, equation (8.19) becomes

$$\frac{(T_{i+2} - T_{i+1})\,4\pi\,r_{i+1}\,K_2}{r_{i+2} - r_i} - \frac{(T_{i+1} - T_i)\,4\pi\,r_i\,K_2}{r_{i+1} - r_{i-1}} + \pi Q(r_{i+1}^2 - r_i^2) = 0\,,$$

using

$$K_{2,r=r_i} = \frac{b_1}{1 + b_2 T_i}$$

and selecting

$$r_i = r_F\sqrt{\frac{i-1}{M}}\,,$$

where M is the number of zones into which the fuel is divided. Each zone thus has the same area and therefore the same power.

Estimating a value for $\bar{T}_f$, the T_i's can be found, and a new $\bar{T}_f$ is calculated from

$$\bar{T}_f = \frac{1}{M}\sum_{i=1}^{M} T_i\,.$$

This continues until convergence has been obtained.

In VOIDN is incorporated the algol procedure TEMP, which carries out the described calculations.

9. HOMOGENIZED BOX CROSS SECTIONS FOR THE OVERALL CALCULATIONS

In this section a description of the methods used for the generation of the macroscopic homogenized few-group cross sections for the overall calculations is given.

The macroscopic homogenized few-group cross sections are constructed on the basis of detailed box calculations performed with the box program

CDB[1]. In principle these box calculations are quite similar to the calculations described in section 5, but the purpose is different.

As a compromise between accuracy and computer time a two-energy-group treatment is used for the three-dimensional overall calculations. As described in section 5 the detailed box calculation is performed in a 5-energy-group structure. These detailed distributed macroscopic 5-group cross sections must be homogenized and condensed to one set of equivalent 2-group cross sections representing the whole box. The principle for this space-energy condensation is to conserve the reaction rates. In the space condensation for each energy group, all cross sections, inclusive of the inverse diffusion constant, i. e. the transport cross section, are flux weighted. In the energy group collapsing, the diffusion constant and the different cross sections are flux weighted.

From a theoretical point of view it is possible to couple the box program and the three-dimensional overall program. This coupling could be established in the same manner as the coupling between the pin cell and the overall calculation in the box program. However, as the box calculations themselves are rather time consuming, such three-dimensional calculations would be prohibitive as regards the computer time. One way to overcome this problem is to precalculate some characteristic two-group cross sections by use of the box program and then interpolate in these cross section tables to get the actual cross sections. This method has been used in the SYNTRON/VOID program for the DRESDEN 1 calculations.

9.1. Construction of the Cross Section Tables

The two-group macroscopic cross sections for the DRESDEN 1 calculations are tabulated in the following way. Naturally, two different types of cross section tables are needed: with and without control rod inserted. The cross sections are tabulated as a function of the burn-up (MWD/TU) and the actual void fraction. However, in section 5 it was shown that the U-depletion and, especially, the Pu-build-up are very sensitive to the average void fraction during the burn-up. This makes it necessary to take into account the average void fraction during the burn-up. As the actual void fraction and the average void fraction during the burn-up history might be different, the following three interpolation, and by that tabulation, parameters should be used: average void during the burn-up, burn-up and actual void.

The box burn-up calculations were accomplished with a fixed void

fraction, the average void fraction, during the burn-up steps. After each burn-up step a few zero timesteps were performed with different void fractions to get cross sections for the actual void fractions. This procedure complicates the calculations, because the change of the void fraction normally requires two or three iterations to make the leakage coupling between the pins and the overall box converge.

Only burn-up between 0 and 10000 MWD/TU was considered, as only the first core was of interest in this case. Burn-up calculations, both with and without control rod inserted, were performed with the average burn-up void fraction at 0%, 25% and 50%. These void fractions were chosen as the average outlet void fraction for the DRESDEN 1 reactor is approximately 47%. As the actual void fractions were expected to be not quite different from the average void, the following actual void fractions were chosen: average void 0%: actual void 0%, 15% and 25%; average void 25%: actual void 15%, 25% and 35%; average void 50%: actual void 35%, 50% and 65%.

These box calculations were set up as simple as justifiable to minimize the necessary computer time. Only six different pin cells are represented in the box. The fission products are treated by one set of equivalent absorption cross sections. The errors introduced by these approximations are discussed in section 5. The buckling in these box calculations was set equal to zero. However, investigations have shown that the influence of the buckling on the resulting two-group cross sections is modest. Two sets of 10-group cross sections were used for each average void fraction: one for the initial calculations and one for the burn-up calculations. The 10-group microscopic pin cell cross sections for the burn-up were generated at 1035 MWD/TU. This procedure is discussed in section 4. To simplify the actual void calculations, the same set of 10-group cross sections and Dancoff factors were used for the different actual void fractions and the average void fraction. This is naturally an approximation; however, as the deviation between the average void and the actual void is maximum 15% void, the accuracy is acceptable, compare the investigations in section 4. The calculation scheme is shown in fig. 9.1.a.

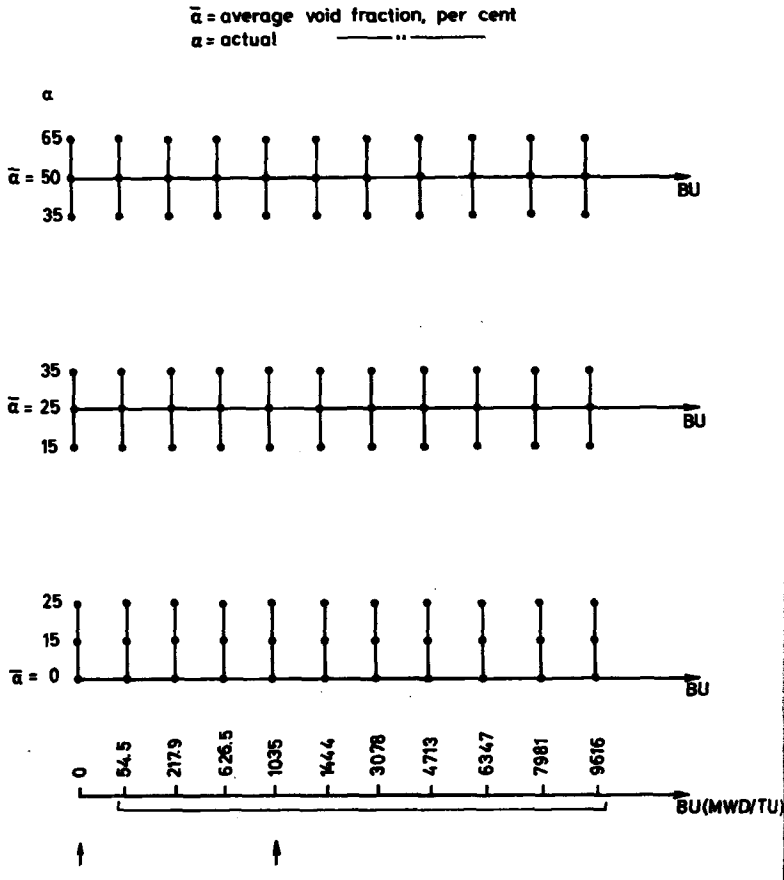

Fig.9.1.a. Calculation scheme for the burn-up tables.

9.2. Fuel Temperature Dependence, Doppler Effect

So far the cross sections have been considered dependent only on the burn-up and the void fraction. However, the temperature has a significant influence on the cross sections, especially the fuel temperature. In these calculations the actual fuel temperature is taken into account by some polynomial corrections to the tabulated cross sections.

A series of runs has been performed with the box program to study the influence of the fuel temperature on the resulting two-group cross sections. Naturally these calculations ought to be performed in the same fashion as the void burn-up tables with average fuel temperature during the burn-up and actual fuel temperature. However, the Doppler effect is only a correction to the burn-up tables and as the fuel temperature in the greater part of the reactor does not change drastically during the burn-up, these fuel temperature investigations were limited to the average fuel temperature during the burn-up.

The average fuel temperature in the DRESDEN 1 reactor is 541 °C. The burn-up tables were generated with this fuel temperature. Box calculations with changed fuel temperature were performed for the void fractions 0%, 25% and 50% and burn-up between 0 and 10000 MWD/TU. For 0% and 50% void the fuel temperature was increased to 1000°C. For 25% void calculations were performed both with fuel temperature at 300° and 1000°C. Analogously with the generation of the burn-up tables, two sets of 10-group microscopic cross sections were applied. The 10-group cross sections were calculated at respectively 0 and 1035 MWD/TU for the specified fuel temperatures. Such box calculations were only accomplished for the box without control rod inserted.

A comparison between the two-group cross sections calculated at the selected fuel temperatures shows that all the different two-group cross sections change with the fuel temperature. However, analysis of the cross sections has shown, as expected, that the changes in the fast absorption cross section and in the removal cross section are of the greatest importance. Originated in spectrum effects, the thermal absorption cross section and the fission cross sections change, but these changes are of such a nature that they nearly neutralize each other. For that reason only the changes in the fast absorption cross section and in the removal cross section are taken into account.

In fig. 9.2.a. and 9.2.b. respectively the fast absorption cross section and the removal cross section are shown as a function of burn-up, void fraction and fuel temperature.

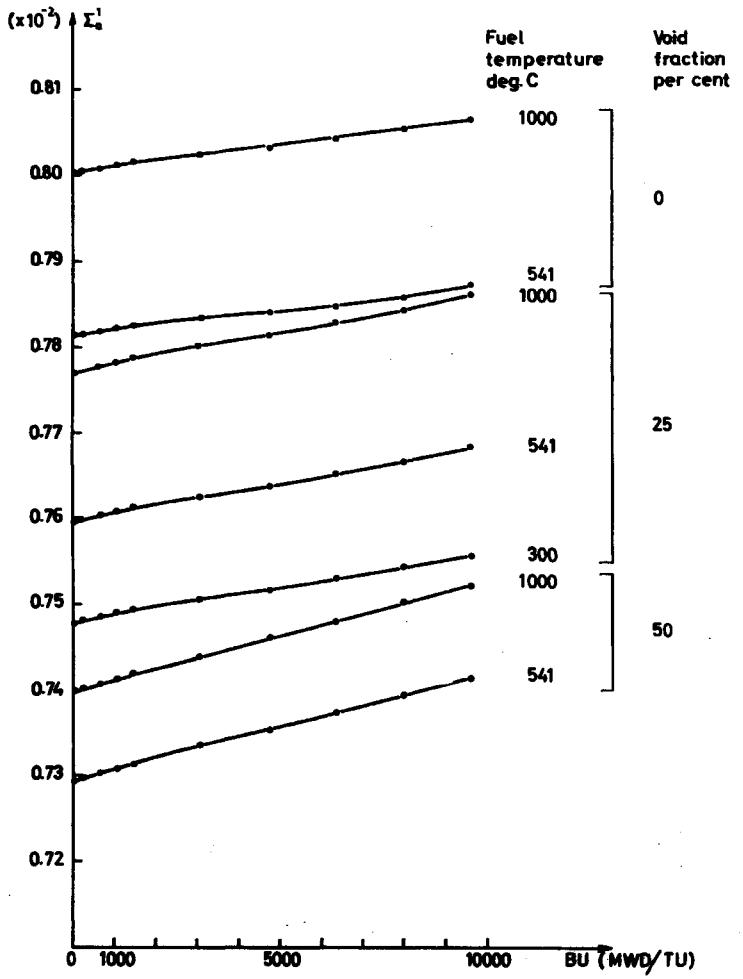

Fig. 9.2.a. DRESDEN 1 box, fast absorption cross section.

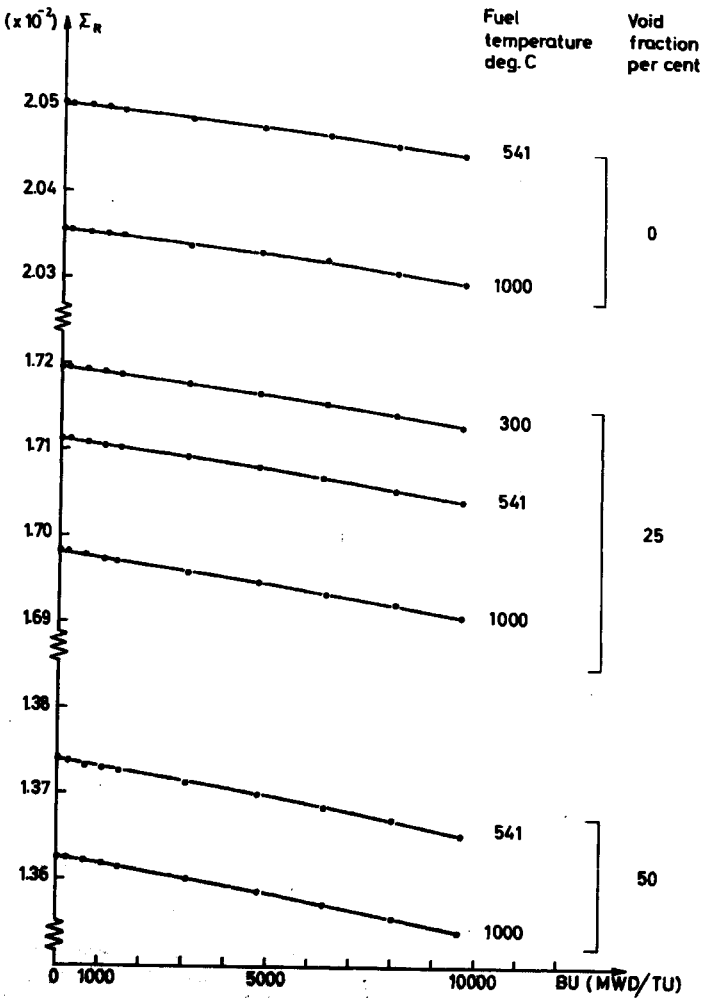

Fig. 9.2.b. DRESDEN 1 box, removal cross section.

On the basis of these curves, Doppler correction polynomials are constructed. For the temperature dependence, the standard square root term is used. As the burn-up dependence is modest, only a polynomial of the first degree is used for the burn-up. The void dependence is more pronounced; for that reason a polynomial of the second degree is used for the void term.

The resulting polynomials have the form shown in section 7, equation (7.2):

$$\Delta\Sigma = (A1 + A2 \cdot BU)\,(1 + A3 \cdot \alpha + A4 \cdot \alpha^2)\,(\sqrt{T} - \sqrt{T_{ref}}) .$$

The calculated polynomial coefficients are shown in table 9.2.a.

Table 9.2.a.

Doppler polynomial coefficients

	A1	A2	A3	A4
Σ_a^1	$2.641_{10}-5$	$8.7_{10}-12$	0.2563	-2.322
Σ_R	$-2.062_{10}-5$	$-3.6_{10}-11$	-0.4342	-0.0434

9.3. Fuel Temperature and Void Coefficients

As a by-product of the cross section calculations described in the previous sections it is possible to obtain some information about the magnitude of the fuel temperature and the void coefficients for the reactor. Naturally reservations must be made as to these results as it is a simplification to determine reactivity coefficients for the whole reactor on the basis of simple box calculations.

On the basis of the average-actual void calculations it is possible to get an estimate on the beginning of life void coefficient. As the average void fraction in the DRESDEN 1 core is approximately 0.25 the void coefficient is calculated as follows:

$$V_c = \frac{k_{eff}(0.25) - k_{eff}(0.35)}{k_{eff}(0.25)} \Big/ 0.1 .$$

The beginning of life Doppler coefficient is calculated in the following way: average void fraction 0.25 and fuel temperatures 541°C and 1000°C.

$$D_c = \frac{k_{eff}(541) - k_{eff}(1000)}{k_{eff}(541)} \Big/ 459 .$$

In table 9.3.a. the calculated coefficients are tabulated.

Table 9.3.a.

Doppler and void coefficients

	V_c	D_c
	$(\Delta k/k)/\Delta v_f$	$(\Delta k/k)/\Delta T$
CDB	-0.066	$-2.3_{10}-5$
Calculated ref. 33	-0.1	$-2.2_{10}-5$

10. 3D OVERALL CALCULATIONS ON THE DRESDEN 1 REACTOR

Different stages of the reactor have been calculated through by the coupled SYNTRON/VOID program by use of the two-group cross section library described in the previous section. Primarily the start-up stages have been investigated in detail, cold clean critical, hot clean critical zero power, hot clean critical full power, and so on, to check the reactivity and the power distribution versus measurements. Great attention has been paid to these start-up situations because they are simple and rather well documented with the control rod positions given. These initial calculations should give a good estimate of the accuracy of the calculations.

Naturally the calculations of greatest interest would be burn-up calculations to give power and exposure distributions during the burn-up. However, such burn-up calculations are very expensive and complicated as the control rod pattern changes almost every day. Moreover, neither the full

control rod management scheme nor detailed measurements are available in the literature. Only the box average exposure distribution end of cycle 1, 5000 MWD/TU, is available, and some simplified calculations. For that reason the 3D burn-up calculations could only be approximative and no direct simulation of cycle 1.

10.1. Initial Calculations, Approach to Criticality

In order to check the accuracy of the calculation methods used, different start situations have been calculated, ranging between the cold clean minimum critical array and the hot clean full power configuration with void. The control rod pattern for these critical configurations are given in ref. 19.

The minimum critical array, cold clean, is shown in fig. 10.1.a. This array was composed of 28 assemblies in the middle of the reactor, with all control rods withdrawn except for one control rod. Reactivity measurements with this control rod at various positions were extrapolated to determine a "rods-out" k_{eff}.

Cold clean box calculations have been performed with the box program CDB to give 2- as well as 5-group macroscopic box cross sections. Static eigenvalue calculations were set up with SYNTRON; the results obtained are shown in fig. 10.1.a. for the "rods-out" situation. The SYNTRON 5-group calculation overestimates k_{eff} by 1.5% and the 2-group calculation by 1.8%. Investigations have shown that only small errors are introduced from the mesh size used in SYNTRON. The mesh size is 3 cm in the core for the 5-group calculation. Box calculations were performed both with the buckling equal to zero and with critical buckling; only small influence on the cross sections was observed.

The problem seems to be that it is not possible to take into account the thermalization from the surrounding reflector in the box calculation. This spectrum effect is very important for such a small reactor configuration.

The start situation calculated next was the fully loaded core, cold clean critical. The control rod pattern shown in fig. 10.1.b. is taken from ref. 19. Fuel and moderator temperatures are equal to 20°C. The control rods are either fully inserted or fully withdrawn. In this overall calculation and all the following ones the neutronics influence of the three spacer zones in the core is neglected to simplify the calculations. This static three-dimensional SYNTRON calculation was set up in 40 x 40 x 40 mesh and 2 energy groups. Only one two-dimensional trial function calculation was performed as this calculation is essentially two-dimensional. The SYNTRON calculation overestimates k_{eff} by 0.8%, compare fig. 10.1.b.

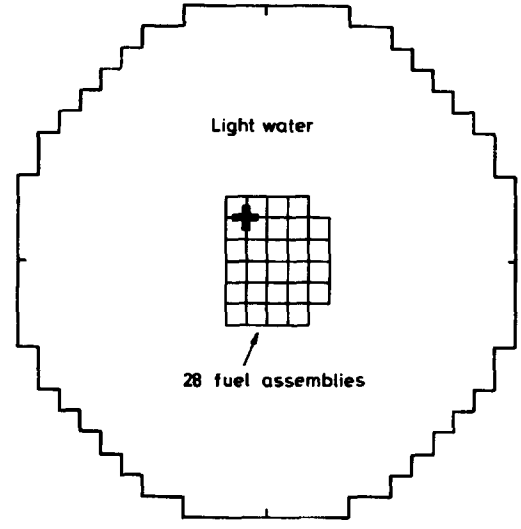

	k_{eff}
SYNTRON 2 energy groups	1.0203
SYNTRON 5 energy groups	1.0171
Measured "rod-out"	1.0022

Fig. 10.1.a. DRESDEN 1, the loading of the minimum critical, 28 fuel assemblies.

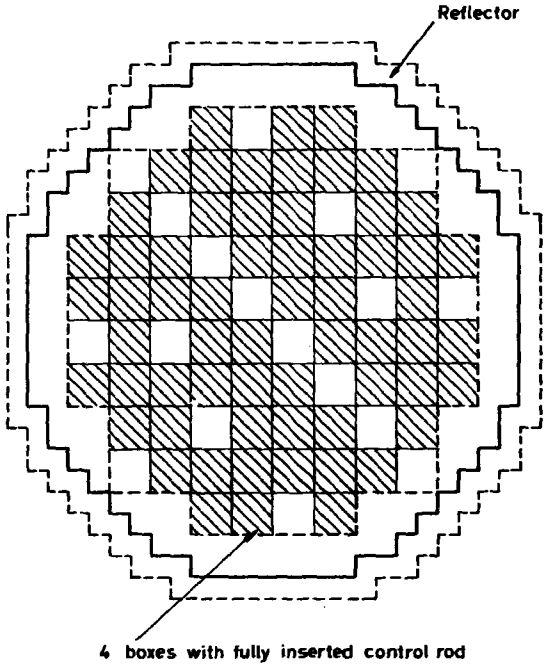

	k_{eff}
SYNTRON 2 groups	1.0080
Measured	1.0000

Fig. 10.1.b. DRESDEN 1, cold clean whole core with control rod pattern.

The reactor start-up was continued by further removal of control rods to raise the temperature to operational temperature and zero power, i.e. the hot clean zero power stage where fuel and moderator temperatures are 284°C. This situation is sketched in fig. 10.1.c. and the control rod pattern is taken from ref. 19. Also here the control rods are either fully inserted or fully withdrawn. In all these calculations 10 cm top and bottom reflectors are used.

A 3D SYNTRON calculation similar to the cold clean case was performed. As no box calculations have been performed with the fuel temperature equal to 284°C, the two-group cross sections from the burn-up table with the fuel temperature equal to 541°C were used. By use of the Doppler correction polynomials these two-group box cross sections were adjusted to the right fuel temperature. In this case, as seen in fig. 10.1.c., k_{eff} is underestimated by approximately 0.4%.

The full power calculations were initiated by some investigations regarding the necessary number of void channels and the importance of the Doppler effect. These investigations were carried out on the unrodded hot clean core. Because of the symmetry only a quarter of the core was used. The SYNTRON/VOID calculations were performed with 24 x 24 mesh in the xy (radial) direction and 36 mesh in the axial direction and 2 energy groups; only two trial functions were used in each group. As top reflector light water with 50% void was used. The reactor core was divided into a number of parallel void channels, each with 10 void points up through the channel. In the coupling between the power distribution and the void distribution, the power calculations are underrelaxated to speed up the convergence. Experience has shown that an underrelaxation factor at about 0.5 is optimal. Convergence criteria are put on the power and void distributions and k_{eff}. Typically 10 power-void iterations are necessary to make the system converge. Besides the void and power, also the temperature distribution is calculated; especially the fuel temperature is used for the Doppler calculations. Such calculations were performed with the reactor divided into 1, 2 and 20 parallel channels plus 1 moderator channel. In table 10.1.a. the calculated form factors and effective multiplication factors are shown.

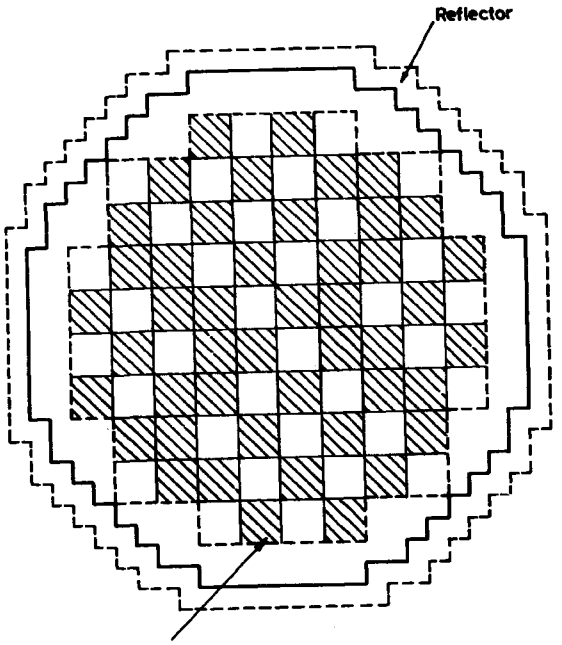

	k_{eff}
SYNTRON 2 groups	0.9957
Measured	1.0000

Fig.10.1.c. DRESDEN 1, hot clean zero power whole core with control rod pattern, fuel temperature = moderator temperature.

Table 10.1.a.

DRESDEN 1, unrodded hot clean

Number of channels	Rad. form fac.	Axial form fac.	k_{eff}
1	2.12	1.87	1.1003
2	1.61	2.32	1.0908
20	1.60	2.54	1.0850

From table 10.1.a. the radial power flattening effect of the void could be observed. As the number of void channels increases k_{eff} decreases, originating from the higher void content in the centre of the core. The axial form factor is observed to increase with the number of void channels. However, this effect is most pronounced for this academic unrodded situation. In the operational situation with control rods inserted in the centre of the core the form factor behaviour is more complex. For the following full power calculations 13 void channels plus 1 moderator channel are chosen.

The significance of the Doppler effect is examined by the one-channel unrodded hot clean calculation. This calculation was repeated with Doppler effect.

Table 10.1.b.

DRESDEN, unrodded hot clean one channel

	Axial form fac.	k_{eff}
Without Doppler	1.87	1.1003
With Doppler	1.75	1.0978

From table 10.1.b. the axial power flattening effect of the Doppler effect could be observed. The Doppler effect decreases the effective multiplication factor, as the power distribution is pressed towards regions with higher void content.

The start-up of the DRESDEN 1 reactor was continued by further removal of control rods from the hot clean zero power stage to raise the power level to full power. In fig. 10.1.d. the hot clean full power control rod pattern taken from ref. 19 is shown. Some of the control rods are left partially withdrawn for axial power flattening. The control rods in DRESDEN 1 have 13 possible notch positions, 0 fully inserted and 12 fully withdrawn. The hot clean full power control rod pattern is not quite symmetric. However, the consumption of computer time would be unacceptably great by full power calculations on the whole core. For that reason an equivalent 1/4 core was used for these calculations. This full power situation was calculated both with the core treated as one void channel and with the 1/4 core divided into 13 parallel void channels. In both cases 24 x 24 mesh in the xy directions and 36 mesh in the axial direction were used for the 2-group flux calculations. Three trial functions in each group were used. Only in the 13-channel case the Doppler effect was accounted for. The calculated effective multiplication factors are shown in fig. 10.1.d. As expected, the 13-channel calculation gives the best result; in this case the deviation between the calculated and the measured k_{eff} is only 0.6%. Unfortunately no power distribution measurements are available for this full power condition. In the next section a power distribution measurement for a hot clean half power situation is described, but only as a box average radial power distribution. However, for the illustration of the behaviour of the axial power, void and fuel temperature distributions for this hot clean full power situation, a typical calculated centre of core axial distribution of these three quantities is shown in fig. 10.1.e. The bump at about 100 cm from the bottom originates from the partially inserted control rods.

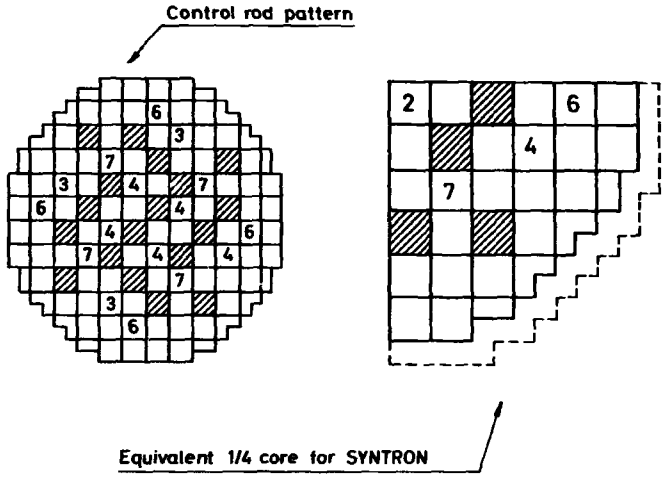

Numbers indicate notch position of partially withdrawn control rods, 0 fully inserted and 12 fully withdrawn.

	k_{eff}
SYNTRON 1 channel no Doppler	1.0150
SYNTRON 13 channels with Doppler	1.0063
Measured	1.0000

Fig. 10.1.d. DRESDEN 1, hot clean full power.

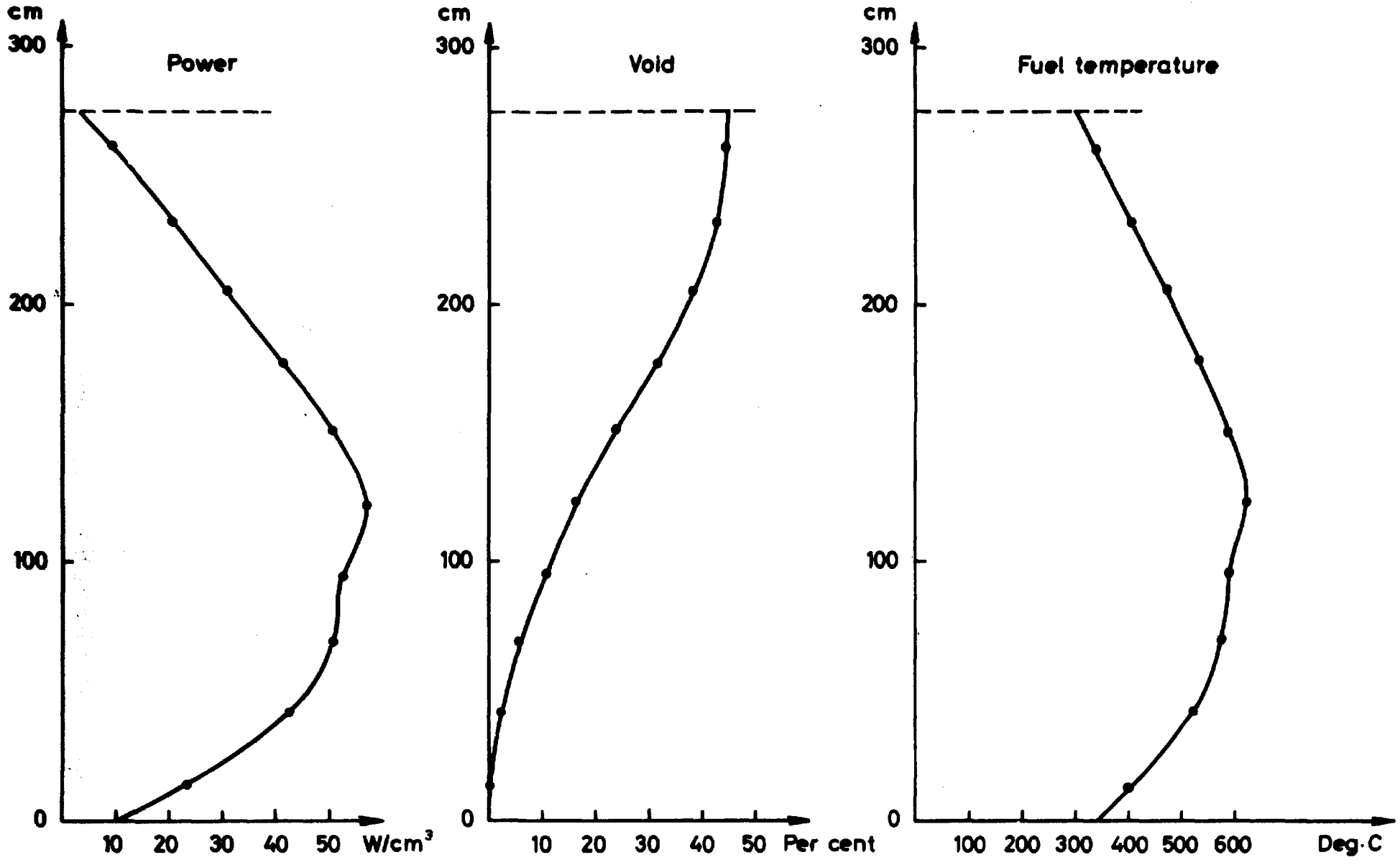

Fig. 10.1.e. DRESDEN 1, axial power, void and fuel temperature distribution centre of core, hot clean full power.

10.2. 3D Burn-up Calculations on the First Cycle of the DRESDEN 1 Reactor

The purpose of generating the cross section burn-up tables described in section 9 was to try to simulate the first cycle of the DRESDEN 1 reactor by use of the SYNTRON/VOID program. Approximations are necessary to overcome such a simulation by use of a time consuming calculation method as that of the SYNTRON/VOID. It is not possible to account for all the small changes during the whole cycle in the quasi-stationary burn-up calculation. One time step takes about half an hour on the Burroughs B 6700 computer at Risø, naturally dependent on the number of void channels and the degree of accuracy in the flux solution. This computer time per. time step is inclusive of 5 to 10 void power iterations.

General Electric has performed such a simulation of the first fuel cycle of DRESDEN 1 to determine the box average exposure distribution at the end of the first cycle at about 5500 MWD/TU. The operating history during the first cycle was divided into ten typical operating control rod configurations, compare ref. 34. None of the control rod patterns is quite symmetric. However, the different control rod patterns are selected in such a way that the effect of the asymmetry is smoothed out during the burn-up. To diminish the necessary computer time the SYNTRON/VOID burn-up calculation was set up on a quarter of the core. In table 10.2.a. the time steps and the quarter core control rod patterns are shown. These quantities are taken from ref. 34.

A measurement of the box average power distribution for the initial half power configuration is reported in ref. 34. A quarter core SYNTRON/VOID calculation with 13 void channels was set up on this configuration. As the control rod pattern was not quite symmetric, one extra, partially inserted, control rod was placed in the centre of the core to account for the asymmetry (A1, 6). The total mass flow was not stated. In the calculation half of full power mass flow was used. In fig. 10.2.a. the calculated and the measured power distributions are shown. The effective multiplication factor k_{eff} is calculated to 1.004. The agreement between the calculated and the measured power distribution is not quite satisfactory. The following conclusions may be drawn from this calculation: for an asymmetric core a quarter core calculation is insufficient; the effect of the control rods in the rest of the core, especially control rods adjacent to unrodded fuel boxes in the selected quarter of the core, may affect the calculated power distribution essentially. It is seen that the calculation generally underestimates the power in boxes with control. This comes from the limited

Table 10.2.a.

Control rod pattern and burn-up scheme for the first cycle of DRESDEN 1.

Time step length (days)	Thermal power (MW)	Burn-up at the end of the step. (MWD/TU)	ΔBU (MWD/TU)	Control rod pattern (compare fig. 2.b.) (Control rod location, notch position) notch position; 0 fully inserted, 12 fully withdrawn.								
13.0	310	78.0	78.0	C1,0	E1,4	A2,5	B2,0	D2,0	B3,2	D3,9	A4,0	C4,0
54.6	620	746.0	668.0	A1,0	D1,2	B2,0	C2,5	A3,0	D3,0	B4,4	A5,6	
27.5	620	1082.0	336.0	C1,0	E1,6	B2,0	D2,3	B3,7	A4,3	C4,0		
16.1	620	1278.0	196.0	C1,0	E1,6	B2,0	D2,3	C3,7	A4,3	C4,1		
64.2	620	2062.0	784.0	A1,0	C1,0	D1,3	B2,3	C3,9	D3,2	B4,0	A5,7	
89.3	620	3153.0	1091.0	C1,5	B2,3	D2,8	C3,0	A4,0	C4,8			
36.4	620	3598.0	445.0	C1,9	B2,3	D2,0	C3,0	A4,2	C4,8			
38.0	620	4062.0	464.0	C1,0	B2,9	C3,5	A4,8					
27.9	620	4403.0	341.0	A1,0	D1,8	C2,0	B3,7					
93.3	620	5543.0	1140.0	A1,2	C2,9	A3,9						

Top : measurement

Bottom : calculation

145	145	110	119 110	61	101 61	99	107 99	108	92 108	73	63 73
135 145	145	110	110	61	61	99	99	108	108	73	73
125	125	70	107 70	93	93	63	95 63	92	92	60	60
113 125	125	70	70	93	93	63	63	92	92	60	60
127	127	98	105 98	103	103	82	82	76	85 76	49	
127	127	98	98	103	103	114 82	82	76	76	49	
97	97	140	109 140	78	78	80	86 80	55	55		
97	97	140	140	78	78	80	80	55			
184	118 184	167	167	113	113	80 64	64				
184	184	167	167	109 113	113	64					
96 141	141	83 113	113	82	82						
69 141	141	113	113								

Average box power 100

Fig.10.2.a. DRESDEN 1, initial half power box average power distribution.

number of void channels used, boxes with and without control rod inserted being put together, which gives too high void in the rodded box and too low void in the unrodded box. The recommendations for future asymmetric core calculations are: full core calculations are necessary, maybe as one-group calculations. Detailed void calculations are necessary, each box must be treated separately. Perhaps better results would be obtained if a more approximative void calculation method be used, which on the other hand allows detailed representation in space.

What may have affected the results of the calculation is the fact that the throttlings in the bottom of the channels are not stated in the literature.

The 3D burn-up calculation was run as a single channel calculation; this was done to diminish the computer time. This simplification is not so severe for the determination of the exposure distribution at the end of the cycle, as the control rods are handled in such a way that all boxes are controlled to the same degree for the whole cycle. The burn-up calculation was performed as a quasi-stationary burn-up calculation with trial function calculations and void-power iterations at the beginning of each time step. The time step lengths, the power level and the control rod patterns for each step are shown in table 10.2.a. Only two trial functions were used in each energy group, but they were recalculated at the beginning of each time step. The number of mesh points in flux solution was 24 x 24 x 36. Besides the Doppler correction, the xenon equilibrium correction was included in this calculation. Ten axial void points were used and the quarter of the reactor core was divided into 300 burn-up regions.

In fig. 10.2.b. the calculated and the measured box average exposure distribution at the end of cycle 1, about 5500 MWD/TU, is shown. The measured exposure distribution is taken from ref. 35. In great parts of the core acceptable agreement between the calculated exposure and the measured one could be observed. In the centre of the core the calculated exposure is too high; this could be expected for a 1-channel treatment as the void content in the centre core is underestimated. In fig. 10.2.c. the effective multiplication factors at the beginning of each times step, with the given control rod pattern, are shown. It is seen that these calculated reactivities during the burn-up in average are rather close to one. The zigzag behaviour may originate from the asymmetric core. Another thing which could affect some of the k_{eff} values is that some of the stated notch positions in ref. 34 are very indistinctly pictured. Unfortunately no three-dimensional power distributions during the first cycle are reported in the literature. However, in ref. 34 a measured axial centre of core power

Top: measurement
Bottom : calculation

154	154	117 144	144	105	113 105	112 113	101 113	122	122	79	79
154	154	144	144	110 105	83 105	107 113	100 113	105 122	122	79	79
106 158	115 158	110	110	102	102	111 109	99 109	92 111	111	66	66
104 158	121 158	110	110	102	102	100 109	105 109	111	111	66	66
109 139	111 139	108 123	109 123	109 99	105 99	95	95	84	84	67 53	
115 139	111 139	115 123	93 123	103 99	99	95	95	84	84	53	
113 113	110 113	112 111	111 111	84	84	79	79	56	56		
104 113	100 113	100 111	94 111	84	84	79	79	56			
100	100	91 101	101	80	82 80	55	55				
100	100	101	101	80	80	55					
64	64	55	55	47	47						
66 64	64	55	55								

Average box exposure 100

Fig. 10.2.b. DRESDEN1, end of the first cycle exposure distribution.

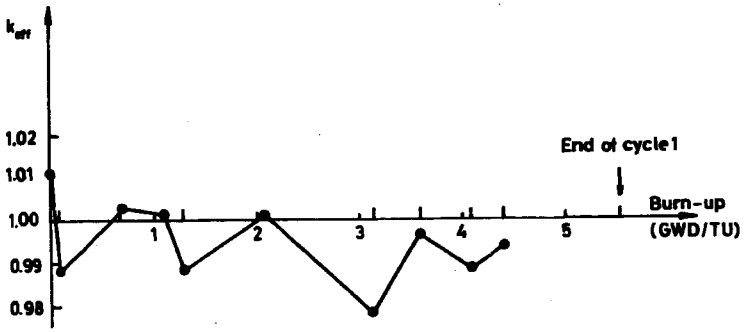

Fig. 10.2.c. k_{eff} versus burn-up, calculated at the beginning of each time step.

form factor at 4000 MWD/TU is reported. The axial form factor is measured to be 1.34; the SYNTRON/VOID calculation gave 1.37.

Unfortunately no further overall measurements are available for the first cycle of the DRESDEN 1 reactor. The conclusion of the burn-up calculation is the same as that mentioned for the initial power distribution calculation: detailed void treatment in space is necessary and whole-core calculations are preferred.

11. CONCLUSION

The following conclusions are drawn from these boiling water reactor investigations. The box burn-up calculations show acceptable agreement with the few available measurements, and this gives some indications of the applicability of the 76-group cross section library. However, the ten energy groups used for the box calculations are too few to allow the same set of ten-group cross sections to be used outside a narrow void interval for which it has been generated. The Y-matrix-representation of the control rod is better than the cross section representation for diffusion theory calculations on the controlled fuel box. The static three-dimensional overall calculations predict with acceptable accuracy the reactivity for the different start-up configurations. The Burroughs B6700 computer at Risø is to small for the detailed calculation method used for full power calculations. Quarter core calculations with only few void channels are unacceptable.

Unfortunately all the available measurements on the DRESDEN 1 reactor are rather integral quantities. More differential measurements are desirable, especially three-dimensional power distribution measurements and box burn-up measurements with the accurate history given.

ACKNOWLEDGEMENTS

The authors wish to thank the members of the Reactor Physics Department at Risø for their assistance; especially our thanks are due to the computer group for the large amount of computer time placed at our disposal.

The continuous help of C. F. Højerup with the box calculations is gratefully appreciated.

REFERENCES

1) K. E. Lindstrøm Jensen, Development and Verification of Nuclear Calculation Methods for Light-Water Reactors. Risø Report No. 235 (1970) 161 pp.

2) A. W. Kramer, Boiling Water Reactors (Addison-Wesley, New York, 1958) 443-499.

3) *Directory of Nuclear Reactors, 4 Power Reactors* (IAEA, Vienna, 1962) 91-96.

4) A. M. Hvidtfeldt Larsen, SIGMA MASTER TAPE, a Multi-group Cross Section Library. Risø Report No. 262 (1972) 50 pp.

5) D. S. Norton, The UKAEA Nuclear Data Library, February 1968. AEEW-M 824 (1968) 23 pp.

6) A. M. Hvidtfeldt Larsen, Risø, Denmark, to be published.

7) C. F. Højerup, Om procedure NELKINSCM til beregning af termiske spredningsdata. Risø-M-1379 (in danish, 1971) (Internal Report) 11 pp.

8) J. Mikkelsen, The Neutron Resonance Reactions in Thermal Nuclear Reactors Determined by Semi-Analytic as well as Numerical Methods. Risø Report No. 234 (1970) 167 pp.

9) J. Mikkelsen and P. Kirkegaard, A User's Guide to the RESAB Program System for the B 6700 Computer. Risø-M-1477 (1972) 53 pp.

10) H. Neltrup, RESOREX, A Procedure for Calculating Resonance Group Cross-Sections. Risø-M-1437 (1971) 25 pp.

11) L. Mortensen, The Fission Product Treatment in the CEB Unit Cell Burn-up Programme. Risø-M-1356 (1971) 69 pp.

12) F. J. Fayers, P. B. Kemshell, and M. J. Terry, An evaluation of some uncertainties in the comparison between theory and experiment for regular light water lattices. J. Brit. Nucl. Energy Soc. 6 (1967) 161-181.

13) C. F. Højerup, Risø, Denmark, unpublished work.

14) M. R. Hackney, D. L. West, and R. Protsik, Isotopic Composition Experiments with Boiling Water Reactor Fuel. In: ANS Topical Meeting-Nuclear Performance of Power-Reactor Cores, San Francisco, 26-27 September 1963 (TID 7672) (USAEC, DTIE, Oak Ridge, Tenn., 1964) 288-302.

15) P. G. Aline et al., Fuel Management and Isotopic Composition Prediction and Experiment in Light Water Power Reactors. In: The Physics Problems in Thermal Reactor Design, Proceedings of an International Conference at the Institution of Civil Engineers, London SW1, 27-29 June 1967. (British Nuclear Energy Society, London, 1967) 297-305.

16) R. Kern and A. T. Shesler, Setup of ISOCHECK Method for determining heavy-isotope content in the operating fuel elements of DRESDEN 1 Core IV. CEND-289 (1967) 117 pp.

17) D. L. Delp et al., FLARE-A Three-Dimensional Boiling Water Reactor Simulator. GEAP-4598 (1964) 95 pp.

18) C. E. Foreman and A. F. Veras, Dresden Refueling and Physics Testing Results. In: ANS Topical Meeting-Nuclear Performance of Power-Reactor Cores, San Francisco, 26-27 September 1963 (TID 7672) (USAEC, DTIE, Oak Ridge, Tenn., 1964) 247-258.

19) A. R. Kosmata and W. R. Kanne, Physics Tests at the DRESDEN Nuclear Power Station. Physics Measurements in Operating Power Reactors. Proceedings of an International Seminar, Rome 9-13 May 1966 (OECD/ENEA, Paris, 1967) 215-263.

20) K. D. Lathrop, User's Guide for the TWOTRAN (x, y) Program, LA 4058 (1968) 23 pp.

21) C. F. Højerup, User's Manual for the Program DIFF 2D. Risø-M-1439 (1971) (Internal Report) 9 pp.

22) J. Pedersen, Calculation of Heterogeneous Constants for Cylinders and Slabs. Risø-M-850 (1969) 23 pp.

23) H. Larsen, SYNTRON, a Three-dimensional Flux Synthesis Program. Risø-M-1346 (1971) 33 pp.

24) S. Kaplan, Some New Methods of Flux Synthesis, Nucl. Sci. Eng. 13 (1962) 22-31.

25) S. Glasstone and M. C. Edlund, The Elements of Nuclear Reactor Theory (D. van Nostrand, New York, 1952) 332.

26) Steen Weber, Xenon-inducerede rumlige effekt oscillationer, Master Thesis, (Danish Atomic Energy Commission, Risø, 1971) (In Danish) 63 pp.

27) H. Larsen, Experience with Flux Synthesis for Burn-up Calculations on Light Water Reactors. IAEA Seminar on Numerical Reactor Calculations, Vienna, 17-21 January 1972, 17 pp.

28) H. Larsen, Risø, Denmark, to be published as Risø Report No. 270.

29) K. Becker, G. Hernborg and M. Bode, An Experimental Study of Pressure Gradients for Flow of Boiling Water in a Vertical Round Duct. Part 1, 2, and 3, AE 69, 70 and 85 (1962) (Aktiebolaget Atomenergi, Sweden).

30) P. Bakstad and K. O. Solberg, A Model for the Dynamics of Nuclear Reactors with Boiling Coolant with a new Approach to the Vapour Generating Process. KR 121 (1967) 68 pp.

31) N. Bech, Risø, Denmark, personal communication (1971).

32) P. T. Hansen and E. Axelsson, HYDRO, A Digital Model for One-Dimensional Time-Dependent Two-Phase Hydrodynamics, AE-RFR 492/RFN 210 (1965). (Internal Reports).

33) R. L. Crowther and D.L. Fischer, Nuclear Characteristics of Large Advanced Boiling Water Reactors. In: ANS Topical Meeting-Nuclear Performance of Power-Reactor Cores, San Francisco, 26-27 September 1963 (TID 7672) (USAEC, DTIE, Oak Ridge, Tenn., 1963) 381-423.

34) C. E. Foreman et al., DRESDEN Cycle 1 Discharged Fuel Exposure and Isotopic Composition Calculations. GECR-4299 (1963) 67 pp.

35) R. J. Mc Whorter and G. R. Parkos, Nuclear Performance of Boiling Water Reactors-An Evaluation of Reactor Operating Data and Reactor Calculations. In: ANS Topical Meeting-Nuclear Performance of Power-Reactor Cores, San Francisco, 26-27 September 1963 (TID 7672) (USAEC, DTIE, Oak Ridge, Tenn., 1963) 71-94.